Motion planning of legged robots

Jean-Daniel Boissonnat, Olivier Devillers, Sylvain Lazard

MOTION PLANNING OF LEGGED ROBOTS*

JEAN-DANIEL BOISSONNAT†, OLIVIER DEVILLERS†, AND SYLVAIN LAZARD‡

Abstract. We study the problem of computing the free space $\mathcal{F}$ of a simple legged robot called the spider robot. The body of this robot is a single point and the legs are attached to the body. The robot is subject to two constraints: each leg has a maximal extension R (accessibility constraint) and the body of the robot must lie above the convex hull of its feet (stability constraint). Moreover, the robot can only put its feet on some regions, called the foothold regions. The free space $\mathcal{F}$ is the set of positions of the body of the robot such that there exists a set of accessible footholds for which the robot is stable. We present an efficient algorithm that computes $\mathcal{F}$ in $O(n^2 \log n)$ time using $O(n^2\alpha(n))$ space for n discrete point footholds where $\alpha(n)$ is an extremely slowly growing function ($\alpha(n) \leqslant 3$ for any practical value of n). We also present an algorithm for computing $\mathcal{F}$ when the foothold regions are pairwise disjoint polygons with n edges in total. This algorithm computes $\mathcal{F}$ in $O(n^2\alpha_8(n)\log n)$ time using $O(n^2\alpha_8(n))$ space ($\alpha_8(n)$ is also an extremely slowly growing function). These results are close to optimal since $\Omega(n^2)$ is a lower bound for the size of $\mathcal{F}$.

Key words. Legged robots, computational geometry, motion planning

AMS subject classifications. 68U05

1. Introduction.

Although legged robots have already been studied in robotics [13, 14], only a very few papers consider the motion planning problem amidst obstacles [8, 7, 1]. In [8, 7] some heuristic approaches are described while, in [1] efficient and provably correct geometric algorithms are described for a restricted type of legged robots, the so-called spider robots to be defined precisely below, and for finite sets of point footholds.

A *legged robot* consists of a body with legs. Each leg has one end attached to the body and the other end (called the foot) that can lie on the ground (or move in space between two positions on the ground). Compared to the classic piano movers problem, legged robots introduce new types of constraints. We assume that the environment consists of regions in the plane, called *foothold regions*, where the robot can safely put its feet. A *foothold* is a point in a foothold region. The legged robot must satisfy two different constraints: the accessibility and the stability constraints. A foothold is said to be *accessible* from a *placement* (position of the body of the robot) if it can be reached by a leg of the robot. A placement is called *stable* if there exist accessible footholds and if the center of mass of the robot lies above the convex hull of these accessible footholds. The set of stable placements is clearly relevant for planning the motion of a legged robot: we call this set *the free space* of the legged robot. Note that a legged robot has at least four legs, three legs ensure the stability of a placement and a fourth leg permits the motion of the robot.

A first simple instance of a legged robot is the *spider robot* (see Figure 1.1). The spider robot was inspired by Ambler, developed at Carnegie Mellon University [9]. The body of the spider robot is a single point in the Euclidean plane and all its legs are attached to the body. The legs are retractable and their lengths may vary between 0 and a constant R. We also assume that the center of mass of the robot is its body.

---

* Part of these results have been presented in conferences [2, 3].

†INRIA Sophia-Antipolis, BP 93, 06902 Sophia Antipolis Cedex, France.
E-mail: firstname.name@sophia.inria.fr. http://www-sop.inria.fr/prisme/prisme_eng.html.

‡INRIA Lorraine, 615 rue du jardin botanique, B.P. 101, 54602 Villers-les-Nancy Cedex, France.
E-mail: lazard@loria.fr. http://www.loria.fr/ lazard/. Most of this work was done while this author was at INRIA Sophia-Antipolis.

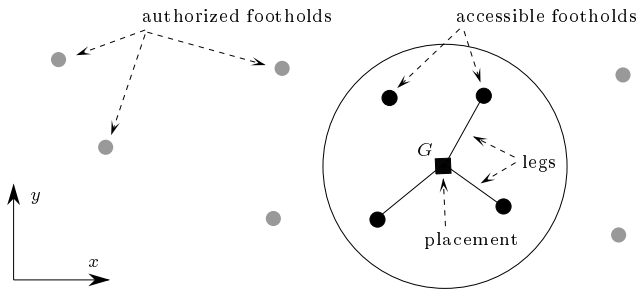

FIG. 1.1. *The spider robot.*

It follows that a placement is stable if the body of the robot lies above the convex hull of the accessible footholds.

The constraint that the body of the spider robot lies in the plane (instead of in 3D) is not really restrictive. Indeed, consider a legged robot for which that constraint is relaxed. Then, if a placement (x, y, z) of such a legged robot is stable then, any placement (x, y, z'), $0 \leqslant z' \leqslant z$ is also stable. Reciprocally, it can be shown that if (x, y) is in the interior of the free space of the spider robot, then there exists $z > 0$ such that (x, y, z) is a stable placement of the corresponding legged robot.

The problem of planning the motion of a spider robot has already been studied by Boissonnat et al. [1]. However, their method assumes that the set of footholds is a finite set of points and cannot be generalized to more complex environments. This paper proposes a new method for computing the free space of a spider robot in the presence of polygonal foothold regions. This method is based on a transformation between this problem and the problem of moving a half-disk amidst obstacles. Our method requires the computation of some parts of the free space of the half-disk. These computations are rather technical and complicated. Consequently, for the sake of clarity, we first present our algorithm for the simple case of discrete footholds, then we show how it can be generalized to the case of polygonal foothold regions.

Once the free space of the spider robot has been computed, it can be used to find trajectories and sequences of legs assignments allowing the robot to move from one point to another. Indeed, once the free space is known, a trajectory of the body can be found in the free space. Then, a sequence of legs assignments can be computed as follows (see [1] for details). Given an initial legs assignment, the body of the robot moves along its trajectory until it crosses the convex hull of its (three) feet that are on the ground or one leg reaches its maximal extension. Then, a suitable foothold is found for the fourth leg and one leg leaves its foothold.

The paper is organized as follows: some notations and results of [1] are recalled in the next section. Section 3 shows the transformation between the spider robot problem and the half-disk problem. We present in Section 4 our algorithm for computing the free space of a spider robot for a discrete set of footholds. Section 5 shows how to extend the algorithm to polygonal foothold regions.

2. Notations and previous results. In Sections 2, 3 and 4, $\mathcal{S}$ denotes a discrete set of distinct footholds $\{s_1, \ldots, s_n\}$ in the Euclidean plane ($\mathcal{S}$ will denote in Section 5 a set of disjoint polygonal regions). Point G denotes the body of the robot (in the same plane) and $[0, R]$ is the length range of each leg. The free space $\mathcal{F}$ is the set of all stable placements of G. A placement is said to be at the *limit of stability* if it lies on the boundary of the convex hull of its accessible footholds. Notice that $\mathcal{F}$ is

a closed set and contains the placements at the limit of stability.

Let C_i denote the circle of radius R centered at s_i. $\mathcal{A}$ is the arrangement of the circles C_i for $1 \leqslant i \leqslant n$, i.e., the subdivision of the plane induced by the circles. This arrangement plays an important role in our problem and we will express the complexity results in term of $|\mathcal{A}|$, the size of $\mathcal{A}$. In the worst-case, $|\mathcal{A}| = \Theta(n^2)$ but if k denotes the maximum number of disks that can cover a point of the plane, among the disks of radius R centered at the s_i, it can be shown that $|\mathcal{A}| = O(kn)$ [15]. Clearly k is not larger than n and in case of sparse footholds, $|\mathcal{A}|$ may be linearly related to the number of footholds.

For any set $\mathcal{E}$, let $\partial(\mathcal{E})$ denote its boundary, $\mathrm{CH}(\mathcal{E})$ its convex hull, $int(\mathcal{E})$ its relative interior[1], $clos(\mathcal{E})$ its closure, and $compl(\mathcal{E})$ its complementary set. Let S^1 denote the set of angles $\mathbb{R}/2\pi\mathbb{Z}$. We denote by $x = y[p]$ the equality of x and y modulo p. We say in the sequel that two objects *properly intersect* if and only if their relative interiors intersect.

The algorithm described in [1] is based on the following observation: for G in a cell Γ of $\mathcal{A}$, the set of footholds that can be reached by the robot is fixed; the portion of Γ that belongs to $\mathcal{F}$ is exactly the intersection of Γ with the convex hull of the footholds that can be reached from Γ. Therefore, the edges of $\partial(\mathcal{F})$ are either circular arcs belonging to $\mathcal{A}$ or portions of line segments joining two footholds. Moreover, a vertex of $\partial(\mathcal{F})$ incident to two straight edges is a foothold (see Figure 2.1). The complexity of $\mathcal{F}$ has been proved to be $|\mathcal{F}| = \Theta(|\mathcal{A}|)$ [1].

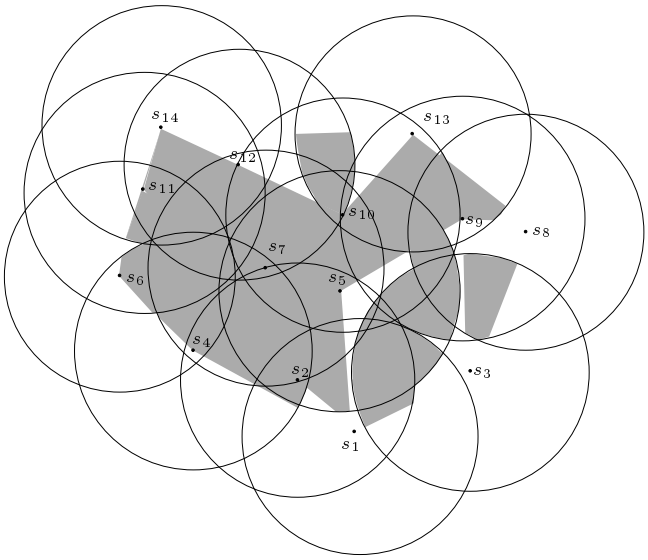

FIG. 2.1. *An example of the free space of a spider robot.*

The algorithm presented in [1] computes the free space $\mathcal{F}$ in $O(|\mathcal{A}| \log n)$ time. It uses sophisticated data structures allowing the off-line maintenance of convex hulls.

The algorithm described in this paper has the same time complexity, uses simple data structures and can be extended to the case where the set $\mathcal{S}$ of footholds is a set

[1] The relative interior of a set $\mathcal{E}$ in a space E is the interior of $\mathcal{E}$ in the space $\mathcal{E}$ for the topology induced by E. For example, the relative interior of a closed line segment in $\mathbb{R}^3$ is the line segment without its endpoints, though its interior in $\mathbb{R}^3$ is empty.

of polygonal regions and not simply a set of points. For simplicity, we consider first the case of point footholds and postpone the discussion on polygonal foothold regions to Section 5.

General position assumption. To simplify the presentation of this paper, we make the following general position assumptions. All these hypotheses can be removed by a careful analysis. Recall that we consider here that the set of footholds is discrete.

No two footholds lie at distance exactly R or $2R$. Among the circles $C_1, \ldots, C_n$ and the line segments joining two footholds, the intersection between three circles or, two circles and a line segment or, one circle and two line segments, is empty.

3. From spider robots to half-disk robots. In this section, we establish the connection between the free space of the spider robot and the free space of a half-disk robot moving by translation and rotation amidst n point obstacles.

THEOREM 3.1. *The spider robot does not admit a stable placement at point P if and only if there exists a half-disk (of radius R) centered at P that does not contain any foothold of $\mathcal{S}$ (see Figure 3.1).*

Proof. Let $\mathcal{R}$ be the set of all the footholds that are reachable from placement P. By definition, P is not stable if and only if the convex hull of $\mathcal{R}$ does not contain P (see Figure 3.1). That is equivalent to say that there exists an open half-plane through P containing $\mathcal{R}$, or that there exists a closed half-disk of radius R centered at P which does not contain any foothold. □

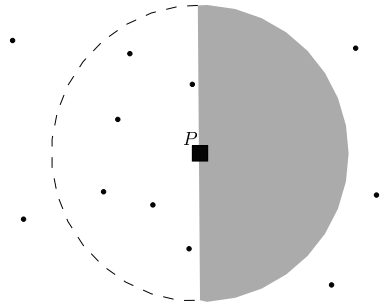

FIG. 3.1. *A placement which is not stable.*

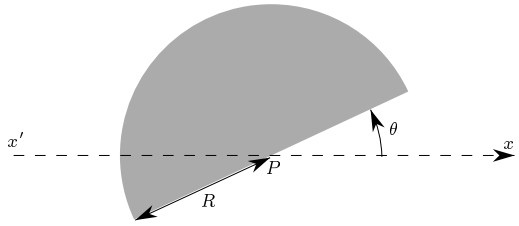

FIG. 3.2. $HD(P, \theta)$.

DEFINITION 3.2. *Let $HD(P, \theta)$ be the half-disk of radius R centered at P (see Figure 3.2) defined by:*

$$\begin{cases} (x - x_P)^2 + (y - y_P)^2 \leqslant R^2 \\ (x - x_P)\sin\theta - (y - y_P)\cos\theta \leqslant 0 \end{cases}$$

DEFINITION 3.3. *$\forall s_i \in \mathcal{S}$ $(1 \leqslant i \leqslant n)$ let:*

$$\mathcal{H}_i = \{(P, \theta) \in I\!R^2 \times S^1 \mid P \in HD(s_i, \theta)\},$$

$$\mathcal{H} = \bigcup_{i=1}^{n} \mathcal{H}_i,$$

$$\mathcal{C}_i = C_i \times S^1.$$

$\mathcal{H}_i$ will be called the helicoidal volume centered at s_i (see Figure 3.3).

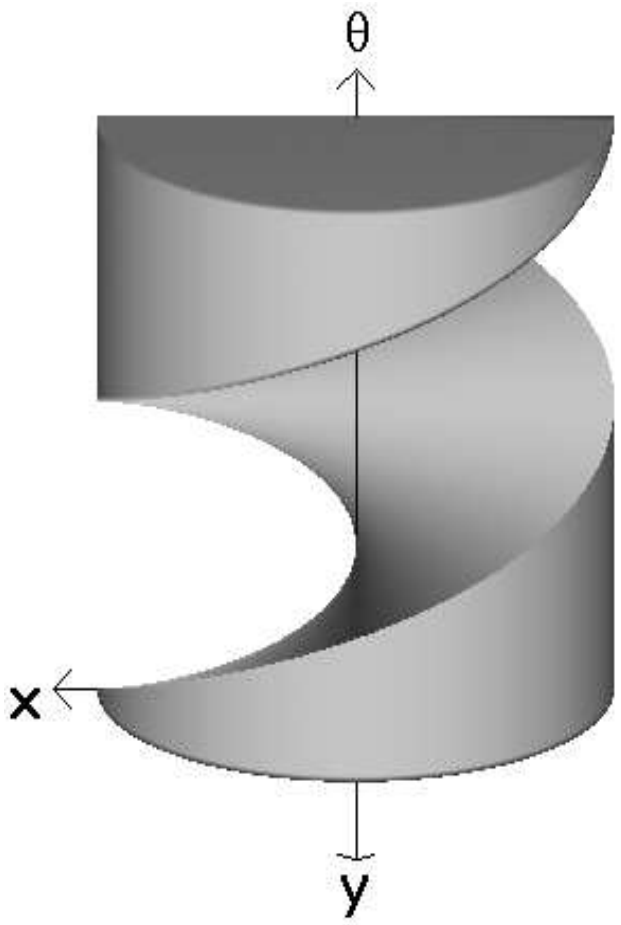

FIG. 3.3. *Helicoidal volume $\mathcal{H}_i$.*

Notice the typographical distinction between the circle C_i defined in $I\!R^2$ and the torus $\mathcal{C}_i$ defined in $I\!R^2 \times S^1$. For convenience, we will often identify S^1 and the interval $[0, 2\pi]$ of $I\!R$. This allows us to draw objects of $I\!R^2 \times S^1$ in $I\!R^3$ and to speak of the θ-axis. Π_{θ_0} denotes the "plane" $\{(P, \theta) \in I\!R^2 \times S^1 \mid \theta = \theta_0\}$.

DEFINITION 3.4. *The free space $\mathcal{L}$ of a half-disk robot moving by translation and rotation amidst the set of obstacles $\mathcal{S}$ is the set of $(P, \theta) \in I\!R^2 \times S^1$ such that the half-disk $HD(P, \theta + \pi)$ does not intersect $\mathcal{S}$.*

PROPOSITION 3.5. $\mathcal{L} = compl(\mathcal{H})$.

Proof. $\forall \theta \in S^1$, the set $\mathcal{L} \cap \Pi_\theta$ is the free space of the half-disk $HD(P, \theta + \pi)$ moving by translation only, amidst the obstacle $s_1, \ldots, s_n$. Since the set of points P such that $HD(P, \theta + \pi)$ contains a s_i is $HD(s_i, \theta)$, $\mathcal{L} \cap \Pi_\theta$ is the complementary set of the union of the $HD(s_i, \theta)$. Thus, $\mathcal{L}$ is the complementary set of the union of the $\mathcal{H}_i$, that is $\mathcal{H}$. □

Let $p_{//\theta}$ denote the mapping (called "orthogonal projection"): $\mathbb{R}^2 \times S^1 \longrightarrow \mathbb{R}^2, (P, \theta) \mapsto P$.

THEOREM 3.6. $\mathcal{F} = compl(p_{//\theta}(compl(\mathcal{H})))$

Proof. By definition of $\mathcal{L}$, $p_{//\theta}(\mathcal{L})$ is the set of points $P \in \mathbb{R}^2$ such that there exists an angle $\theta \in S^1$ such that the half-disk $HD(P, \theta)$ does not intersect $\mathcal{S}$. By Theorem 3.1, it is equivalent to say that there exists $\theta \in S^1$ such that $HD(P, \theta)$ does not intersect $\mathcal{S}$, or that P is not a stable placement of the spider robot. Thus, $p_{//\theta}(\mathcal{L})$ is the set of points P where the robot does not admit a stable placement, i.e., $\mathcal{F} = compl(p_{//\theta}(\mathcal{L}))$. The result then follows from Proposition 3.5. □

REMARK 3.7. $compl(p_{//\theta}(compl(\mathcal{H}))) \times S^1$ is the largest "cylinder" included in $\mathcal{H}$, whose axis is parallel to the θ-axis (in grey in Figure 3.4). The basis of this cylinder is $\mathcal{F}$.

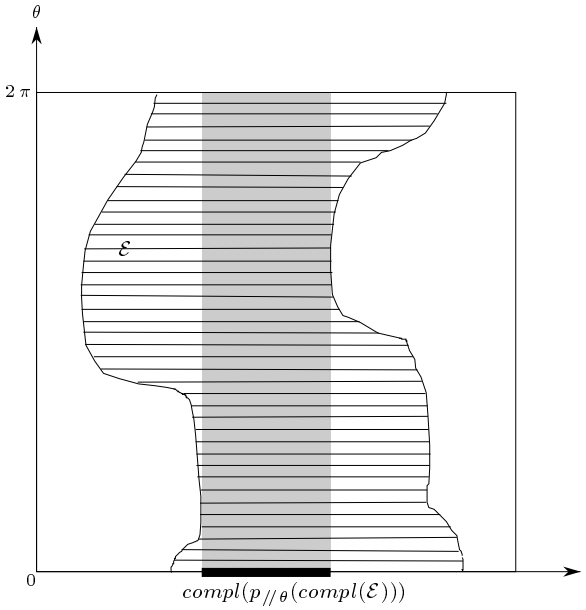

FIG. 3.4. $compl(p_{//\theta}(compl(\mathcal{E})))$.

REMARK 3.8. The results of this section do not depend on the fact that the footholds are discrete points. For more general foothold regions, we simply need to replace the helicoidal volumes by their analog. This will be done in Section 5.

4. Computation of $\mathcal{F}$. In this section, we propose an algorithm for computing $\mathcal{F}$ based on Theorem 3.6.

A first attempt to use Theorem 3.6 may consist in computing $\mathcal{L} = compl(\mathcal{H})$ and projecting it onto the horizontal plane. The motion planning of a convex polygonal robot in a polygonal environment has been extensively studied (see for example [10,

11]). Such algorithms can be generalized to plan the motion of a half-disk. It should lead to an algorithm of complexity $O(n\lambda_s(n)\log n)$, where $\lambda_s(n)$ is an almost linear function of n. The projection can be done using classical techniques, such as projecting all the faces of $\mathcal{L}$ and computing their union. Since the complexity of the 3D object $\mathcal{L}$ is not directly related to the complexity of its projection, this approach does not provide a combinatorial bound on $\mathcal{F}$. However, assuming $|\mathcal{F}| = O(\lambda_s(|\mathcal{A}|))$ (which will be proved in this paper) the time complexity of the algorithm of Kedem et al. is $O(n\lambda_s(n)\log n + \lambda_s(|\mathcal{A}|)\log^2 n)$.

In this paper, we present a direct computation of $\mathcal{F}$. This approach provides an upper bound on the size of $\mathcal{F}$, namely $|\mathcal{F}| = O(\lambda_s(|\mathcal{A}|))$. It also provides an algorithm for computing $\mathcal{F}$ in $O(\lambda_s(|\mathcal{A}|)\log n)$ time. As in [16] and contrary to [11], the algorithm proposed here is sensitive to $|\mathcal{A}|$ which is usually less than quadratic. Another advantage of our direct computation is to avoid the explicit construction of the 3D object $\mathcal{L}$ which is useless for our application. Our algorithm manipulates only two-dimensional arrangements or lower envelopes and we provide a detailed description of the curves involved in the construction.

Let us now detail the computation of $\mathcal{F}$ in the case of point footholds. We know that each arc of the boundary $\partial(\mathcal{F})$ of $\mathcal{F}$ is either a straight line segment belonging to a line joining two footholds or an arc of a circle C_i (see Section 2). The circular arcs $\partial(\mathcal{F}) \cap C_i$ are computed first (Sections 4.1, 4.2 and 4.3) and linked together with the line segments in a second step (Sections 4.4 and 4.5).

4.1. Computation of $\partial(\mathcal{F}) \cap \mathcal{A}$. In the sequel, the *contribution* of an object X to another object Y is $X \cap Y$. We compute the contribution of each circle C_{i_0}, $i_0 = 1, \ldots, n$, to $\partial(\mathcal{F})$ in turn. Recall that $\mathcal{C}_{i_0}$ denote the torus $C_{i_0} \times S^1$. The contribution of each circle C_{i_0} to $\partial(\mathcal{F})$ will be obtained by computing the intersection of all the $\mathcal{H}_i$, $i = 1, \ldots, n$, with the torus $\mathcal{C}_{i_0}$. Let $\mathcal{Z}_i$, $i = 1, \ldots, n$, denote these intersections:

$$\mathcal{Z}_i = \mathcal{H}_i \cap \mathcal{C}_{i_0}.$$

We first show how to compute the contribution of C_{i_0} to $\partial(\mathcal{F})$ in term of the $\mathcal{Z}_i$, and leave the studies of the shape and properties of $\mathcal{Z}_i$ to Section 4.2. Figures 4.1 and 4.2 show some (hatched) $\mathcal{Z}_i \subset \mathcal{C}_{i_0}$ $(i \neq i_0)$ where $\mathcal{C}_{i_0}$ is parameterized by (u, θ) (u and θ parameterize C_{i_0} and S^1 respectively); the dark grey region shows $\mathcal{Z}_{i_0}$.

PROPOSITION 4.1. *The contribution of C_{i_0} to $\partial(\mathcal{F})$ is:*

$$C_{i_0} \cap \partial(\mathcal{F}) = compl(p_{//\theta}(compl(\cup_i \mathcal{Z}_i))) \setminus int(compl(p_{//\theta}(compl(\cup_{i \neq i_0} \mathcal{Z}_i)))).$$

Proof. Since $\mathcal{F}$ is a closed set, $C_{i_0} \cap \partial(\mathcal{F}) = [C_{i_0} \cap \mathcal{F}] \setminus [C_{i_0} \cap int(\mathcal{F})]$. According to Theorem 3.6, $\mathcal{F} = compl(p_{//\theta}(compl(\mathcal{H})))$. One can easily prove that for any set $\mathcal{E} \in I\!R^2 \times S^1$, $int(compl(\mathcal{E})) = compl(clos(\mathcal{E}))$, $clos(compl(\mathcal{E})) = compl(int(\mathcal{E}))$, and $clos(p_{//\theta}(\mathcal{E})) = p_{//\theta}(clos(\mathcal{E}))$. It then follows from the expression of $\mathcal{F}$ that $int(\mathcal{F}) = compl(p_{//\theta}(compl(int(\mathcal{H}))))$.

Recall that for any sets $X, Y \in I\!R^2 \times S^1$, $compl(X \cap Y) = compl(X) \cup compl(Y)$, $p_{//\theta}(X \cup Y) = p_{//\theta}(X) \cup p_{//\theta}(Y)$, and $compl(X \cup Y) = compl(X) \cap compl(Y)$. That implies

$$compl(p_{//\theta}(compl(X \cap Y))) = compl(p_{//\theta}(compl(X))) \cap compl(p_{//\theta}(compl(Y))).$$

We now consider that equation with X equal to $\mathcal{H}$ or $int(\mathcal{H})$, and Y equal to the torus $\mathcal{C}_{i_0}$. Since $compl(p_{//\theta}(compl(\mathcal{C}_{i_0})))$ is the circle C_{i_0} we get:

$$compl(p_{//\theta}(compl(\mathcal{H} \cap \mathcal{C}_{i_0}))) = \mathcal{F} \cap C_{i_0} \text{ and}$$
$$compl(p_{//\theta}(compl(int(\mathcal{H}) \cap \mathcal{C}_{i_0}))) = int(\mathcal{F}) \cap C_{i_0}.$$

Since $\mathcal{H} = \cup_{i=1}^n \mathcal{H}_i$ and $\mathcal{Z}_i = \mathcal{H}_i \cap \mathcal{C}_{i_0}$ by definition, $\mathcal{H} \cap \mathcal{C}_{i_0} = \cup_{i=1}^n \mathcal{Z}_i$ and

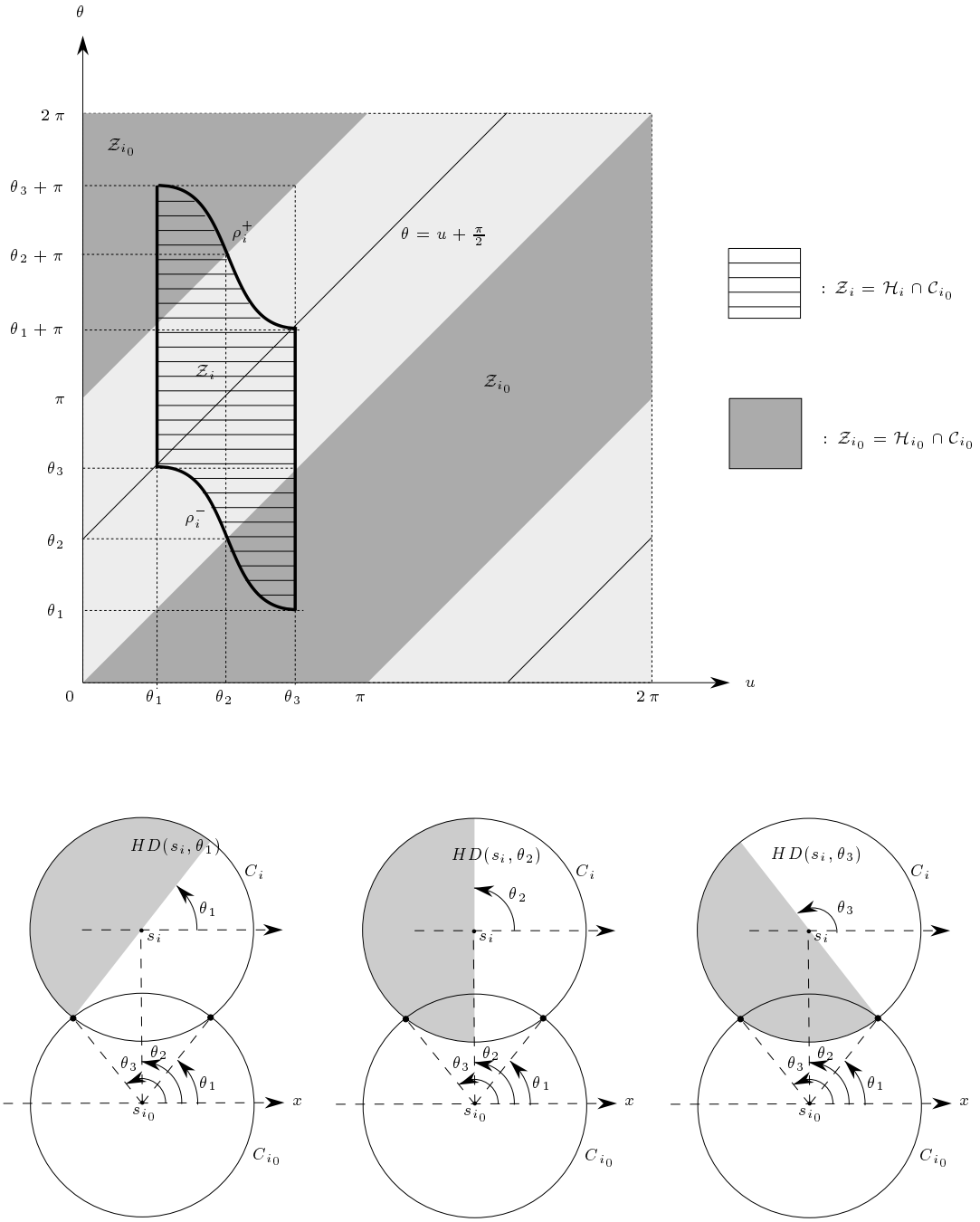

FIG. 4.1. *Example of $\mathcal{Z}_i$ for $\|s_{i_0} s_i\| = \sqrt{2}\,R$ and some corresponding critical positions of $HD(s_i, \theta)$.*

$int(\mathcal{H}) \cap \mathcal{C}_{i_0} = \cup_{i=1}^{n}(int(\mathcal{H}_i) \cap \mathcal{C}_{i_0})$. By the general position assumption, no two footholds lie at distance $2R$, thus for $i \neq i_0$, $int(\mathcal{H}_i) \cap \mathcal{C}_{i_0} = int(\mathcal{Z}_i)$[2]. As $int(\mathcal{H}_{i_0}) \cap \mathcal{C}_{i_0} = \emptyset$, we get $int(\mathcal{H}) \cap \mathcal{C}_{i_0} = \cup_{i \neq i_0} int(\mathcal{Z}_i)$. The study of the shape of $\mathcal{Z}_i$ will yield (see Lemma 4.8) that $\cup_{i \neq i_0} int(\mathcal{Z}_i) = int(\cup_{i \neq i_0} \mathcal{Z}_i)$. Therefore, $int(\mathcal{F}) \cap C_{i_0} = compl(p_{//\theta}(compl(int(\cup_{i \neq i_0} \mathcal{Z}_i)))) = int(compl(p_{//\theta}(compl(\cup_{i \neq i_0} \mathcal{Z}_i))))$ and $\mathcal{F} \cap C_{i_0} = compl(p_{//\theta}(compl(\cup_i \mathcal{Z}_i)))$. Using $C_{i_0} \cap \partial(\mathcal{F}) = [C_{i_0} \cap \mathcal{F}] \setminus [C_{i_0} \cap int(\mathcal{F})]$, we get the result. □

Thus, the contribution of C_{i_0} to $\partial(\mathcal{F})$ comes from the computation of $\cup_i \mathcal{Z}_i$ and $\cup_{i \neq i_0} \mathcal{Z}_i$.

Geometrically, $compl(p_{//\theta}(compl(\cup_i \mathcal{Z}_i)))$ is the vertical projection (along the θ-axis) of the largest vertical strip Σ_{i_0} included in $\cup_i \mathcal{Z}_i$ (see Figure 4.2). Similarly, $compl(p_{//\theta}(compl(\cup_{i \neq i_0} \mathcal{Z}_i)))$ is the projection of the largest vertical strip Σ'_{i_0} included in $\cup_{i \neq i_0} \mathcal{Z}_i$. Thus, $\partial(\mathcal{F}) \cap C_{i_0}$ is the vertical projection onto C_{i_0} of the vertical strip $\Sigma_{i_0} \setminus int(\Sigma'_{i_0})$.

In order to compute $\mathcal{F}$ efficiently, we need to compute the union of the regions $\mathcal{Z}_i$ efficiently. More precisely, we will show that the union of the regions $\mathcal{Z}_i$ can be computed in $O(k_{i_0} \log k_{i_0})$ time where k_{i_0} is the number of helicoidal volumes $\mathcal{H}_i$ intersecting $\mathcal{C}_{i_0}$.

This is possible because the $\mathcal{Z}_i$ have special shapes that allow us to reduce the computation of their union to the computation of a small number of lower envelopes of curves drawn on $\mathcal{C}_{i_0}$, with the property that two of them intersect at most once. The geometric properties of the $\mathcal{Z}_i$ are discussed in Section 4.2 and, in Section 4.3, we present and analyze the algorithm for constructing $\partial(\mathcal{F}) \cap C_{i_0}$.

4.2. Properties of the $\mathcal{Z}_i$. We study here the regions $\mathcal{Z}_i = \mathcal{H}_i \cap \mathcal{C}_{i_0}$. Recall that we parameterize $\mathcal{C}_{i_0} = C_{i_0} \times S^1$ by (u, θ) where u and θ parameterize C_{i_0} and S^1 respectively ($u = 0$ corresponds to the point of C_{i_0} with maximum x-coordinate). Figures 4.1 and 4.2 show examples of such regions $\mathcal{Z}_i$. For convenience, we will use the vocabulary of the plane when describing objects on the torus $\mathcal{C}_{i_0}$. For instance, the curve drawn on the torus $\mathcal{C}_{i_0}$ with equation $a\,\theta + b\,u + c = 0$ will be called a line. The line $u = u_0$ will be called vertical and oriented according to increasing θ. Lower and upper will refer to this orientation. The discussion below considers only non empty regions $\mathcal{Z}_i$ (such that $\|s_{i_0} s_i\| < 2R$).

We introduce first some notations. Let $HC_i(\theta)$ be the half-circle of the boundary of $HD(s_i, \theta)$, i.e., $HC_i(\theta) = C_i \cap HD(s_i, \theta)$. Let $r_i(\theta)$ be the spoke of C_i that makes an angle θ with the x-axis, i.e., $r_i(\theta) = \{s_i + \lambda \vec{u}_\theta \mid \lambda \in [0, R]\}$ where $\vec{u}_\theta$ is the unit vector whose polar angle is θ. The boundary of $\mathcal{H}_i$ is composed of the three following patches:

$$\begin{aligned} \mathcal{T}_i &= \{(HC_i(\theta), \theta) \in I\!R^2 \times S^1\} \\ \mathcal{R}_i^+ &= \{(r_i(\theta), \theta) \in I\!R^2 \times S^1\} \\ \mathcal{R}_i^- &= \{(r_i(\theta + \pi), \theta) \in I\!R^2 \times S^1\} \end{aligned}$$

Let ρ_i^- and ρ_i^+ denote the curves $\mathcal{R}_i^- \cap \mathcal{C}_{i_0}$ and $\mathcal{R}_i^+ \cap \mathcal{C}_{i_0}$, respectively. Since $\mathcal{R}_i^-$ and $\mathcal{R}_i^+$ are translated copies of one another, i.e., $\mathcal{R}_i^- = \mathcal{R}_i^+ \pm (0, 0, \pi)$, we have:

LEMMA 4.2. *ρ_i^- and ρ_i^+ are translated copies of one another, i.e.,*
$\rho_i^+ = \{(u, \theta) \in S^1 \times S^1 \mid (u, \theta - \pi) \in \rho_i^-\} = \{(u, \theta) \in S^1 \times S^1 \mid (u, \theta + \pi) \in \rho_i^-\}$.

[2] Recall that int denotes the relative interior, thus $int(\mathcal{H}_i)$ is the interior of $\mathcal{H}_i$ in $I\!R^2 \times S^1$ but $int(\mathcal{Z}_i)$ denotes the interior of $\mathcal{Z}_i$ in $\mathcal{C}_{i_0}$.

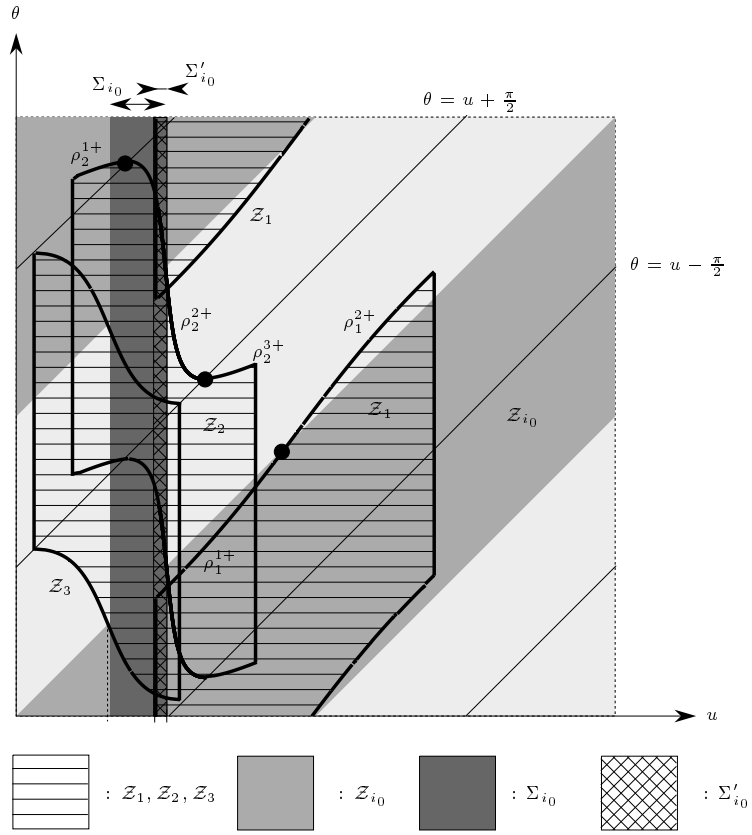

FIG. 4.2. *Contribution of C_{i_0} to $\partial(\mathcal{F})$ ($0 < \|s_1 s_{i_0}\| < R$, $R \leqslant \|s_2 s_{i_0}\| < \sqrt{2}R$, $\sqrt{2}R \leqslant \|s_3 s_{i_0}\| < 2R$).*

LEMMA 4.3. *The curves $\rho_i^{\pm}$ are monotone in u.*

Proof. Assume for a contradiction that a curve $\rho_i^{\pm}$ is not monotone in u. Then, there exists u and $\theta \neq \theta'$ in S^1 such that (u, θ) and (u, θ') parameterize points of $\rho_i^{\pm}$. By the definition of $\mathcal{R}_i^{\pm}$, it then follows that the point $U \in C_{i_0}$ parameterized by u belongs to the two spokes $r_i(\theta)$ (or $r_i(\theta+\pi)$) and $r_i(\theta')$ (or $r_i(\theta'+\pi)$). The intersection between any two of these spokes is exactly s_i. Thus, $U = s_i$, which contradicts (since $U \in C_{i_0}$) the general position assumption saying that the distance between s_i and s_{i_0} is not R. □

LEMMA 4.4. *The region $\mathcal{Z}_{i_0}$ is the subset of $\mathcal{C}_{i_0}$ parameterized by $\{(u, \theta) \in S^1 \times S^1 \mid \theta \leqslant u \leqslant \theta + \pi\}$ (shown in grey in Figures 4.1 and 4.2).*

Proof. For any $\theta \in S^1$, the intersection between $\mathcal{H}_{i_0}$ and the "horizontal plane" Π_θ is the half-disk $HD(s_{i_0}, \theta)$. Similarly, the intersection between $\mathcal{C}_{i_0}$ and that plane is C_{i_0}. Thus, the intersection between $\mathcal{Z}_{i_0}$ and Π_θ is $HC_{i_0}(\theta)$, which is parameterized on C_{i_0} by $\{u \in S^1 \mid \theta \leqslant u \leqslant \theta + \pi\}$. That intersection is actually on the plane Π_θ and is therefore parameterized on $\mathcal{C}_{i_0}$ by $\{(u, \theta) \in S^1 \times S^1 \mid \theta \leqslant u \leqslant \theta + \pi\}$. □

PROPOSITION 4.5. *$\mathcal{Z}_i$ is a connected region bounded from below by ρ_i^- and from above by ρ_i^+, i.e., $\mathcal{Z}_i = \{(u, \theta) \in S^1 \times S^1 \mid \exists x \in [0, \pi], (u, \theta - x) \in \rho_i^-, (u, \theta - x + \pi) \in \rho_i^+\}$ (see Figures 4.1, 4.2).*

Proof. By cutting $\mathcal{C}_{i_0}$ and $\mathcal{H}_i$ by the "horizontal plane" Π_θ, we get that a point

parameterized by (u,θ) on $\mathcal{C}_{i_0}$ belongs to $\mathcal{H}_i$ if and only if the point U parameterized by u on C_{i_0} belongs to $HD(s_i,\theta)$. Since $HD(s_i,\theta)$ can be seen as the union of the spokes $\{r_i(\theta+\gamma) \mid \gamma \in [0,\pi]\}$, $(u,\theta) \in \mathcal{Z}_i$ if and only if there exists $\gamma \in [0,\pi]$ such that $U \in r_i(\theta+\gamma)$, or equivalently, $U \in r_i(\theta - x + \pi)$ with $x = \pi - \gamma \in [0,\pi]$. Since $\mathcal{R}_i^- = \{(r_i(\theta - x + \pi), \theta - x) \mid \theta - x \in S^1\}$, it follows from $U \in r_i(\theta - x + \pi)$ that the point of $\mathcal{C}_{i_0}$ parameterized by $(u, \theta - x)$ belongs to $\mathcal{R}_i^-$ and thus to $\rho_i^- = \mathcal{R}_i^- \cap \mathcal{C}_{i_0}$. From Lemma 4.2, we get that the point parameterized by $(u, \theta - x + \pi)$ belongs to ρ_i^+. Therefore, $\mathcal{Z}_i$ is a connected region bounded from below by ρ_i^- and from above by ρ_i^+. □

We want to compute the union of the $\mathcal{Z}_i$ by computing the "lower envelope"[3] of the lower edges ρ_i^-, and the "upper envelope" of the upper edges ρ_i^+. It is unfortunately impossible to do so because some upper edges ρ_i^+ may possibly be "below" or intersect some lower edges ρ_j^-. However, we can subdivide the regions $\mathcal{Z}_i$ into blocks $\mathcal{Z}_i^k$, $k \in \mathcal{K}$, and separate these blocks into two sets Ω_1 and Ω_2 such that the union of the $\mathcal{Z}_i^k$ in Ω_1 (resp. Ω_2) is the region bounded from above by the upper envelope of the upper edges of the $\mathcal{Z}_i^k \in \Omega_1$ and bounded from below by the lower envelope of the lower edges of the $\mathcal{Z}_i^k \in \Omega_1$ (resp. Ω_2). Such property can be realized by showing that all the upper edges of the $\mathcal{Z}_i^k \in \Omega_1$ belong to the strip $\{(u,\theta) \in S^1 \times [u + \frac{\pi}{2}, u + \frac{3\pi}{2}]\}$ and all the lower edges of the $\mathcal{Z}_i^k \in \Omega_1$ belong to the strip $\{(u,\theta) \in S^1 \times [u - \frac{\pi}{2}, u + \frac{\pi}{2}]\}$ (a similar property is shown for Ω_2). Note that the upper and lower envelopes are then defined since they are considered in $S^1 \times \mathbb{R}$.

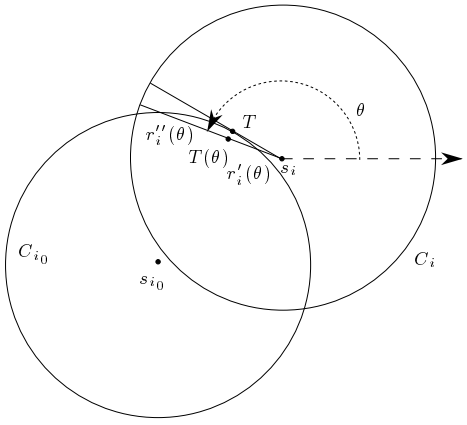

FIG. 4.3. *For the definition of $r_i'(\theta)$ and $r_i''(\theta)$.*

We subdivide $\mathcal{Z}_i$ into blocks $\mathcal{Z}_i^k$ when $R < \|s_{i_0}s_i\| < \sqrt{2}\,R$. That subdivision is performed such that the upper and lower edges of the $\mathcal{Z}_i^k$ are θ-monotone. Recall that the upper edge ρ_i^+ of $\mathcal{Z}_i$ is the intersection of $\mathcal{R}_i^+ = \{(r_i(\theta),\theta) \mid \theta \in S^1\}$ and $\mathcal{C}_{i_0}$. The spoke $r_i(\theta)$ intersects C_{i_0} twice (for some θ) when $R < \|s_{i_0}s_i\| < \sqrt{2}\,R$, which implies that ρ_i^+ is not θ-monotone. We cut the spoke $r_i(\theta)$ into two pieces such that each piece intersects C_{i_0} at most once. Let T be the intersection point between C_{i_0} and on one of the two lines passing through s_i and tangent to C_{i_0} (see Figure 4.3). Let $T(\theta)$ be the point on $r_i(\theta)$ at distance $\|s_iT\|$ from s_i. Cutting $r_i(\theta)$ at $T(\theta)$ defines two sub-spokes $r_i'(\theta)$ and $r_i''(\theta)$ that intersect C_{i_0} in at most one point each; without loss of generality, let $r_i'(\theta)$ denote the sub-spoke joining s_i to

[3] Note that the lower and upper envelopes of curves in $S^1 \times S^1$ are not actually defined.

$T(\theta)$. The set of $\theta \in S^1$ for which $r'_i(\theta)$ intersects C_{i_0} is clearly connected but the set of $\theta \in S^1$ for which $r''_i(\theta)$ intersects C_{i_0} consists of two connected components. We denote by ρ_i^{2+} the intersection $\{(r'_i(\theta), \theta) \mid \theta \in S^1\} \cap \mathcal{C}_{i_0}$ and by ρ_i^{1+} and ρ_i^{3+} the two connected components of the intersection $\{(r''_i(\theta), \theta) \mid \theta \in S^1\} \cap \mathcal{C}_{i_0}$ (see Figure 4.2). Since $r'_i(\theta)$ and $r''_i(\theta)$ intersect C_{i_0} at most once for any $\theta \in S^1$, the curves ρ_i^{1+}, ρ_i^{2+} and ρ_i^{3+} are θ-monotone. The lower edges ρ_i^{k-}, $k = 1, 2, 3$ can be defined similarly or in a simpler way as the translated copies of ρ_i^{k+}, $k = 1, 2, 3$, i.e., $\rho_i^{k-} = \{(u, \theta) \in S^1 \times S^1 \mid (u, \theta + \pi) \in \rho_i^{+k}\}$. We denote by $\mathcal{Z}_i^k$, $k = 1, 2, 3$, the subset of $\mathcal{Z}_i$ bounded from above by ρ_i^{k+} and from below by ρ_i^{k-}.

We can now prove the following proposition that will allow us to compute the union of the $\mathcal{Z}_i$ by computing the upper and lower envelopes of their upper and lower edges.

PROPOSITION 4.6. *If $0 \leqslant \|s_{i_0} s_i\| < R$, the line $\theta = u - \frac{\pi}{2}$ properly intersects $\mathcal{Z}_i$, and the lines $\theta = u \pm \frac{\pi}{2}$ properly intersect neither ρ_i^+ nor ρ_i^-.*

If $R < \|s_{i_0} s_i\| < \sqrt{2}\, R$, the line $\theta = u + \frac{\pi}{2}$ properly intersects $\mathcal{Z}_i^2$, and the line $\theta = u - \frac{\pi}{2}$ properly intersects $\mathcal{Z}_i^1$ and $\mathcal{Z}_i^3$. Furthermore, the lines $\theta = u \pm \frac{\pi}{2}$ properly intersect none of the edges ρ_i^{1+}, ρ_i^{1-}, ρ_i^{2+}, ρ_i^{2-}, ρ_i^{3+} and ρ_i^{3-}.

If $\sqrt{2}\, R \leqslant \|s_{i_0} s_i\| < 2R$, the line $\theta = u + \frac{\pi}{2}$ properly intersects $\mathcal{Z}_i$, and the lines $\theta = u \pm \frac{\pi}{2}$ properly intersect neither ρ_i^+ nor ρ_i^-.

Proof. Let (u_P, θ_P) parameterize a point of a curve ρ_i. Let P denote the point of C_{i_0} with parameter u_P and $\gamma = \angle(\overrightarrow{Ps_{i_0}}, \overrightarrow{Ps_i})$ $[2\pi]$ (see Figure 4.4). One can easily show that $\gamma = \theta_P - u_P[\pi]$. We prove that $\gamma \neq \frac{\pi}{2}$ $[\pi]$, except possibly when (u_P, θ_P) is an endpoint of ρ_i (or ρ_i^k when $R < \|s_{i_0} s_i\| < \sqrt{2}\, R$), which implies, since $\gamma = \theta_P - u_P[\pi]$, that the lines $\theta = u \pm \frac{\pi}{2}$ intersect neither ρ_i^+ nor ρ_i^- (resp. ρ_i^{k+} nor ρ_i^{k-}), except possibly at their endpoints.

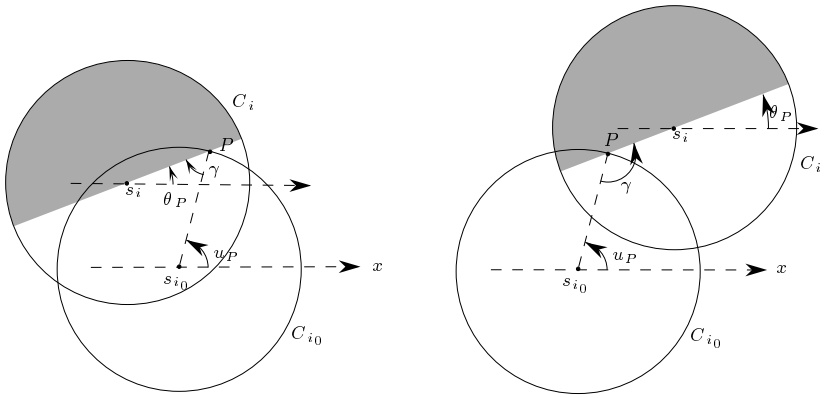

FIG. 4.4. *For the proof of Proposition 4.6.*

Case 1: $0 \leqslant \|s_{i_0} s_i\| < R$. Since s_i belongs to the disk of radius R centered at s_{i_0}, $\gamma \in (-\frac{\pi}{2}, \frac{\pi}{2})$ for any $P \in C_{i_0}$ (see Figure 4.4). Thus, the lines $\theta = u \pm \frac{\pi}{2}$ properly intersect neither ρ_i^+ nor ρ_i^-. Finally, the point of $\mathcal{C}_{i_0}$ $(\theta_2, \theta_2 - \frac{\pi}{2})$, where $\theta_2 = \angle(\vec{x}, \overrightarrow{s_{i_0} s_i})$ $[2\pi]$, belongs to the line $\theta = u - \frac{\pi}{2}$ and also to the relative interior of $\mathcal{Z}_i$ since it belongs to the interior of $\mathcal{H}_i$ (see Figure 4.5a). Therefore, the line $\theta = u - \frac{\pi}{2}$ properly intersects $\mathcal{Z}_i$.

Case 2: $R < \|s_{i_0} s_i\| < \sqrt{2}\, R$. Let (u_{P_1}, θ_{P_1}) parameterize the point connecting ρ_i^{1+} and ρ_i^{2+}, and (u_{P_2}, θ_{P_2}) parameterize the point connecting ρ_i^{2+} and ρ_i^{3+}. Let P_1

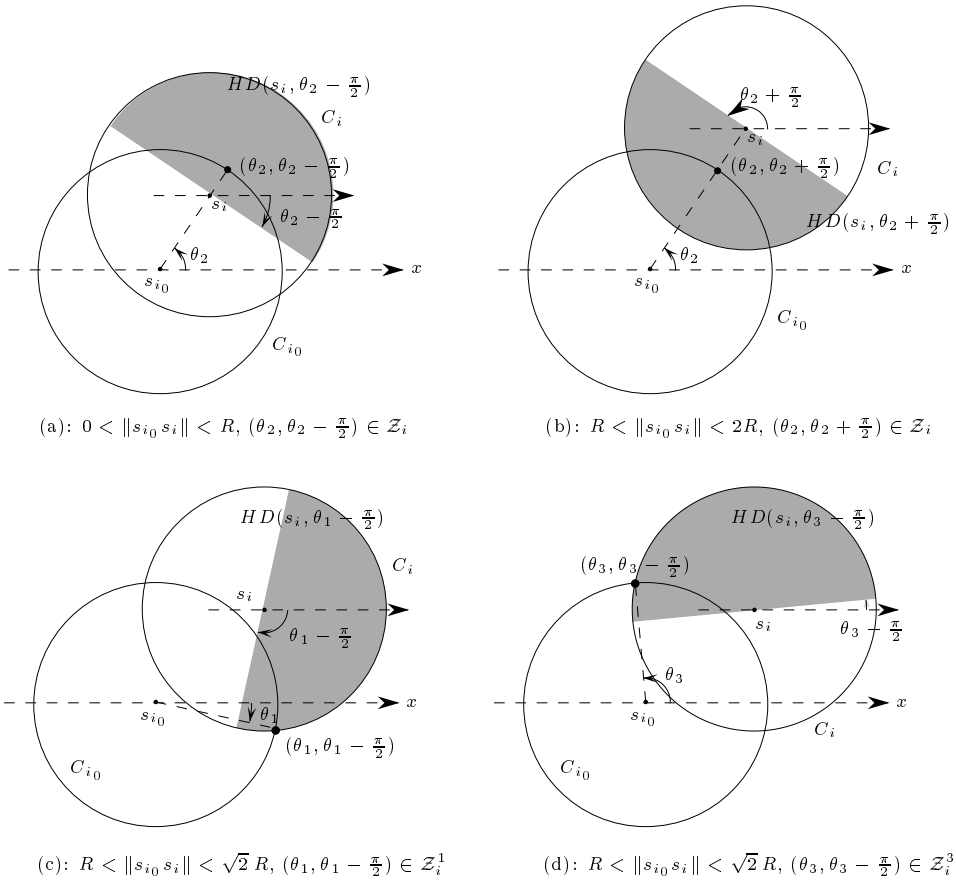

(a): $0 < \|s_{i_0} s_i\| < R$, $(\theta_2, \theta_2 - \frac{\pi}{2}) \in \mathcal{Z}_i$

(b): $R < \|s_{i_0} s_i\| < 2R$, $(\theta_2, \theta_2 + \frac{\pi}{2}) \in \mathcal{Z}_i$

(c): $R < \|s_{i_0} s_i\| < \sqrt{2}\, R$, $(\theta_1, \theta_1 - \frac{\pi}{2}) \in \mathcal{Z}_i^1$

(d): $R < \|s_{i_0} s_i\| < \sqrt{2}\, R$, $(\theta_3, \theta_3 - \frac{\pi}{2}) \in \mathcal{Z}_i^3$

FIG. 4.5. *For the proof of Proposition 4.6: section of $\mathcal{H}_i$ and $\mathcal{C}_{i_0}$ by the "planes" $\Pi_{\theta_2 - \frac{\pi}{2}}$, $\Pi_{\theta_2 + \frac{\pi}{2}}$, $\Pi_{\theta_1 - \frac{\pi}{2}}$ and $\Pi_{\theta_3 - \frac{\pi}{2}}$ respectively.*

and P_2 denote the points of C_{i_0} parameterized by u_{P_1} and u_{P_2} respectively. According to the construction of ρ_i^{1+}, ρ_i^{2+} and ρ_i^{3+}, the tangent lines to C_{i_0} at P_1 and P_2 pass through s_i. At most two tangent lines to C_{i_0} pass through s_i, thus P_1 and P_2 are the only points of C_{i_0} where $\gamma = \frac{\pi}{2}\ [\pi]$. Since ρ_i^+ is u-monotone by Lemma 4.3, (u_{P_1}, θ_{P_1}) and (u_{P_2}, θ_{P_2}) are the only points of ρ_i^+ where $\gamma = \frac{\pi}{2}\ [\pi]$. Therefore, the lines $\theta = u \pm \frac{\pi}{2}$ do not properly intersect ρ_i^{k+}, $k = 1, 2, 3$. Similarly, the lines $\theta = u \pm \frac{\pi}{2}$ do not properly intersect ρ_i^{k-}, $k = 1, 2, 3$.

Let θ_1 and θ_3 be the parameters on C_{i_0} of the intersection points between C_{i_0} and C_i (see Figures 4.5c and d); to differentiate θ_1 from θ_3, assume without loss of generality that, for any $\varepsilon > 0$ small enough, the points of C_{i_0} parameterized by $\theta_1 + \varepsilon$ and $\theta_3 - \varepsilon$ are in the disk of radius R centered at s_i. Then, the points $(\theta_1, \theta_1 - \frac{\pi}{2})$ and $(\theta_3, \theta_3 - \frac{\pi}{2})$ of $\mathcal{C}_{i_0}$ belong to $\mathcal{Z}_i^1$ and $\mathcal{Z}_i^3$ (or to $\mathcal{Z}_i^3$ and $\mathcal{Z}_i^1$) respectively (see Figures 4.5c and d). However, these points do not belong to the relative interior of $\mathcal{Z}_i^1$ and $\mathcal{Z}_i^3$ (because they lie on the border of $HD(s_i, \theta_1 - \frac{\pi}{2})$ and $HD(s_i, \theta_3 - \frac{\pi}{2})$). Nevertheless, there clearly exists $\varepsilon > 0$ small enough such that the point parameterized by $\theta_1 + \varepsilon$ (resp. $\theta_3 - \varepsilon$) on C_{i_0} belongs to the interior of the half-disk $HD(s_i, \theta_1 - \frac{\pi}{2} + \varepsilon)$ (resp. $HD(s_i, \theta_3 - \frac{\pi}{2} - \varepsilon)$). Thus, the points $(\theta_1 + \varepsilon, \theta_1 + \varepsilon - \frac{\pi}{2})$ and $(\theta_3 - \varepsilon, \theta_3 - \varepsilon - \frac{\pi}{2})$

of $\mathcal{C}_{i_0}$ belong to the relative interior of $\mathcal{Z}_i^1$ and $\mathcal{Z}_i^3$ respectively. Therefore, the line $\theta = u - \frac{\pi}{2}$ properly intersects $\mathcal{Z}_i^1$ and $\mathcal{Z}_i^3$.

On the other hand, $(\theta_2, \theta_2 + \frac{\pi}{2})$ (where $\theta_2 = \angle(\vec{x}, \overrightarrow{s_{i_0} s_i})\ [2\pi]$) belongs to relative interior of $\mathcal{Z}_i^2$ because the point of C_{i_0} parameterized by θ_2 belongs to the relative interior of the sub-spoke $r_i'(\theta_2 + \pi)$ (see Figure 4.5b) which belongs to interior of $HD(s_i, \theta_2 + \frac{\pi}{2})$. Therefore, the line $\theta = u + \frac{\pi}{2}$ properly intersects $\mathcal{Z}_i^2$.

Case 3: $\sqrt{2}\,R \leqslant \|s_{i_0} s_i\| < 2R$. Since $r_i(\theta)$ intersects C_{i_0} at most once, $\gamma \in [\frac{\pi}{2}, \frac{3\pi}{2}]$ (see Figure 4.4). Moreover, $\gamma = \frac{\pi}{2}\ [\pi]$ only when $\|s_{i_0} s_i\| = \sqrt{2}\,R$, but then, P is at distance R from s_i which implies that (u_P, θ_P) is an endpoint of ρ_i. Thus, the lines $\theta = u \pm \frac{\pi}{2}$ intersect neither ρ_i^+ nor ρ_i^-, except possibly at their endpoints. Finally, the point $(\theta_2, \theta_2 + \frac{\pi}{2})$ of $\mathcal{C}_{i_0}$ (where $\theta_2 = \angle(\vec{x}, \overrightarrow{s_{i_0} s_i})\ [2\pi]$) belongs to the line $\theta = u + \frac{\pi}{2}$ and also to the relative interior of $\mathcal{Z}_i$ (see Figures 4.5b and 4.1). Therefore, the line $\theta = u + \frac{\pi}{2}$ properly intersects $\mathcal{Z}_i$. □

By Proposition 4.6, we can compute the union $\cup_{i \neq i_0} \mathcal{Z}_i$ by separating the $\mathcal{Z}_i$, $\mathcal{Z}_i^k$ into two sets Ω_1 and Ω_2 (where $\mathcal{Z}_i$, $\mathcal{Z}_i^k$ belongs to Ω_1 if and only if ρ_i^+, ρ_i^{k+} belongs to the strip $\{(u, \theta) \in S^1 \times [u + \frac{\pi}{2}, u + \frac{3\pi}{2}]\}$ and ρ_i^-, ρ_i^{k-} belongs to the strip $\{(u, \theta) \in S^1 \times [u - \frac{\pi}{2}, u + \frac{\pi}{2}]\}$) and computing the union of the $\mathcal{Z}_i$, $\mathcal{Z}_i^k$ in Ω_1 (resp. Ω_2) by computing the upper envelope of their upper edges and the lower envelope of their lower edges. In order to compute efficiently these upper and lower envelopes, we show that the curves ρ_i^+, ρ_i^-, ρ_i^{k+} and ρ_i^{k-} intersect each other at most once. However, we need for that purpose to split the regions $\mathcal{Z}_i$ when $0 < \|s_{i_0} s_i\| < R$ into two blocks $\mathcal{Z}_i^1$ and $\mathcal{Z}_i^2$ separated by the vertical line $u = \theta_2 = \angle(\vec{x}, \overrightarrow{s_{i_0} s_i})$; it also remains to split the θ-interval (or the u-interval) over which ρ_i is defined into two intervals of equal length over which $\rho_i^{1\pm}$ and $\rho_i^{2\pm}$ are defined (see Figure 4.2). Note that Proposition 4.6 still holds if we replace (when $0 < \|s_{i_0} s_i\| < R$) $\mathcal{Z}_i$ by $\mathcal{Z}_i^k$ and $\rho_i^\pm$ by $\rho_i^{k\pm}$, $k = 1, 2$.

For consistency, we split $\mathcal{Z}_{i_0}$ into two blocks $\mathcal{Z}_{i_0}^1$ and $\mathcal{Z}_{i_0}^2$ separated by a vertical line (chosen arbitrarily, say $u = \pi$). Also for consistency, the curves $\rho_i^\pm$ when $\sqrt{2}\,R \leqslant \|s_{i_0} s_i\| < 2R$ are occasionally denoted in the sequel $\rho_i^{1\pm}$.

LEMMA 4.7. *Let ρ_i' and ρ_j' be some connected portions of $\rho_i^\pm$ and $\rho_j^\pm$ respectively ($i \neq j$). If ρ_i' or ρ_j' is monotone in θ and defined over a θ-interval smaller than π, then ρ_i' and ρ_j' intersect at most once.*

Proof. Let (u_I, θ_I) be a point of intersection between ρ_i' and ρ_j' and I be the point of the circle C_{i_0} with parameter u_I. Since ρ_i' is a portion of the intersection between $\mathcal{C}_{i_0}$ and $\mathcal{R}_i^\pm$, I is a point of intersection between C_{i_0} and the diameter of $HD(s_i, \theta_I)$. Therefore, the line passing through s_i and I has slope θ_I.

By applying the same argument to ρ_j', we obtain that s_i and s_j belong to the same straight line of slope θ_I. Therefore, if ρ_i' and ρ_j' intersect twice, at (u_I, θ_I) and (u_J, θ_J), then $\theta_I = \theta_J[\pi]$. It follows, if ρ_i' or ρ_j' is defined over a θ-interval smaller than π, that $\theta_I = \theta_J[2\pi]$. Furthermore, if ρ_i' or ρ_j' is monotone in θ, then (u_I, θ_I) and (u_J, θ_I) are equal. □

LEMMA 4.8. $\forall i, j,\ int(\mathcal{Z}_i) \cup int(\mathcal{Z}_j) = int(\mathcal{Z}_i \cup \mathcal{Z}_j)$.

Proof. We assume that $i \neq j$ because otherwise the result is trivial. One can easily show that $int(\mathcal{Z}_i) \cup int(\mathcal{Z}_j) \neq int(\mathcal{Z}_i \cup \mathcal{Z}_j)$ only if the boundaries of $\mathcal{Z}_i$ and $\mathcal{Z}_j$ partially coincide, i.e., the dimension of $\partial(\mathcal{Z}_i) \cap \partial(\mathcal{Z}_j)$ is 1.

By Proposition 4.5, $\partial(\mathcal{Z}_i)$ consists of the edges ρ_i^+ and ρ_i^- and of two vertical line segments joining the endpoints of ρ_i^+ and ρ_i^- when these endpoints exist (which is the case when $i \neq i_0$). Moreover, these vertical line segments are clearly supported by the vertical lines $u = \theta_1$ and $u = \theta_3$ where θ_1 and θ_3 parameterize on C_{i_0} the points of intersection between C_{i_0} and C_i (see Figure 4.1).

By Lemma 4.7, the edges $\rho_i^{\pm}$ and $\rho_j^{\pm}$ do not partially coincide. By the general position assumption, no three distinct circles C_{i_0}, C_i and C_j have a common intersection point. Thus, for any $i \neq j$, $C_{i_0} \cap C_i$ and $C_{i_0} \cap C_j$ are disjoint. Therefore, the vertical lines $\partial(\mathcal{Z}_i) \setminus \{\rho_i^+, \rho_i^-\}$ and $\partial(\mathcal{Z}_j) \setminus \{\rho_j^+, \rho_j^-\}$ do not partially coincide. Finally, since $\rho_i^{\pm}$ is nowhere partially supported by a vertical line by Lemma 4.3, $\rho_i^{\pm}$ and the vertical lines $\partial(\mathcal{Z}_j) \setminus \{\rho_j^+, \rho_j^-\}$ do not partially coincide. □

PROPOSITION 4.9. *Any two curves among the curves $\rho_i^{k\pm}$ intersect at most once (where $k \in \{1,2\}$ if $0 \leqslant \|s_{i_0}s_i\| < R$, $k \in \{1,2,3\}$ if $R < \|s_{i_0}s_i\| < \sqrt{2}\,R$, and $k = 1$ if $\sqrt{2}\,R \leqslant \|s_{i_0}s_i\| < 2R$).*

Proof. By Lemma 4.7, it is sufficient to prove that all the curves $\rho_i^{k\pm}$, $i \neq i_0$, are monotone in θ and defined over θ-intervals smaller than π. Indeed, the curves $\rho_{i_0}^{1+}$, $\rho_{i_0}^{1-}$, $\rho_{i_0}^{2+}$ and $\rho_{i_0}^{2-}$ clearly do not pairwise intersect more than once, by Lemma 4.4.

If $0 < \|s_{i_0}s_i\| < R$, any spoke of C_i intersects C_{i_0} at most once. Hence, $\rho_i^{\pm}$ is monotone in θ. $\rho_i^{\pm}$ is defined over a θ-interval greater than π but smaller than 2π. Since we have split that interval in two equal parts, $\rho_i^{1\pm}$ and $\rho_i^{2\pm}$ are defined over a θ-interval smaller than π (see $\mathcal{Z}_1$ in Figure 4.2).

If $R < \|s_{i_0}s_i\| < \sqrt{2}\,R$, the θ-interval where $r_i(\theta)$ (or $r_i(\theta+\pi)$) intersects C_{i_0} is smaller than π, which implies that ρ_i is defined over a θ-interval smaller than π. The curves ρ_i^{k+}, $k = 1,2,3$, are defined as the connected components of $\{(r_i'(\theta),\theta) \mid \theta \in S^1\} \cap \mathcal{C}_{i_0}$ and $\{(r_i''(\theta),\theta) \mid \theta \in S^1\} \cap \mathcal{C}_{i_0}$. Since the sub-spokes $r_i'(\theta)$ and $r_i''(\theta)$ intersect C_{i_0} at most once for any $\theta \in S^1$, the curves ρ_i^{k+}, $k = 1,2,3$, are θ-monotone.

If $\sqrt{2}\,R \leqslant \|s_{i_0}s_i\| < 2R$, $r_i(\theta)$ (and also $r_i(\theta+\pi)$) intersects C_{i_0} in at most one point, which proves that ρ_i is monotone in θ. Furthermore, the θ-interval where ρ_i is defined is smaller than π because the θ-interval where $r_i(\theta)$ (or $r_i(\theta+\pi)$) intersects C_{i_0} is smaller than π. □

4.3. Construction of $\partial(\mathcal{F}) \cap C_{i_0}$. We first show how to compute $\cup_i \mathcal{Z}_i$. Let Ω_1 and Ω_2 be the following sets of $\mathcal{Z}_i^k$:

$$\Omega_1 = \{\mathcal{Z}_i \mid \sqrt{2}\,R \leqslant \|s_{i_0}s_i\| < 2R\} \cup \{\mathcal{Z}_i^2 \mid R < \|s_{i_0}s_i\| < \sqrt{2}\,R\},$$
$$\Omega_2 = \{\mathcal{Z}_i^1, \mathcal{Z}_i^2 \mid 0 \leqslant \|s_{i_0}s_i\| < R\} \cup \{\mathcal{Z}_i^1, \mathcal{Z}_i^3 \mid R < \|s_{i_0}s_i\| < \sqrt{2}\,R\}.$$

By Proposition 4.6, the line $\theta = u + \frac{\pi}{2}$ properly intersects all the $\mathcal{Z}_i^k \in \Omega_1$ but the lines $\theta = u \pm \frac{\pi}{2}$ properly intersect none of their upper and lower edges ρ_i^{k+} and ρ_i^{k-}. Thus, the regions $\mathcal{Z}_i^k \in \Omega_1$ can be seen as regions of $\{(u,\theta) \in S^1 \times [u - \frac{\pi}{2}, u + \frac{3\pi}{2}]\}$ such that all their upper edges ρ_i^{k+} lie in $\{(u,\theta) \in S^1 \times [u + \frac{\pi}{2}, u + \frac{3\pi}{2}]\}$ and all their lower edges ρ_i^{k-} lie in $\{(u,\theta) \in S^1 \times [u - \frac{\pi}{2}, u + \frac{\pi}{2}]\}$. Therefore, the union of the $\mathcal{Z}_i^k \in \Omega_1$ is the region of $\{(u,\theta) \in S^1 \times [u - \frac{\pi}{2}, u + \frac{3\pi}{2}]\}$ bounded from above by the upper envelope of their ρ_i^{k+} and bounded from below by the lower envelope of their ρ_i^{k-}. Similarly, the union of the $\mathcal{Z}_i^k \in \Omega_2$ is the region of $\{(u,\theta) \in S^1 \times [u - \frac{3\pi}{2}, u + \frac{\pi}{2}]\}$ bounded from above by the upper envelope of the ρ_i^{k+} and bounded from below by the lower envelope of the ρ_i^{k-}.

The union of Ω_1 and Ω_2, which is $\cup_i \mathcal{Z}_i$, can be achieved by computing, on one hand, the intersection between the upper edge chain of $\cup_{\mathcal{Z}_i^k \in \Omega_1} \mathcal{Z}_i^k$ with the lower edge chain of $\cup_{\mathcal{Z}_i^k \in \Omega_2} \mathcal{Z}_i^k$ (which both belong to $\{(u,\theta) \in S^1 \times S^1 \mid \theta \in [u + \frac{\pi}{2}, u + \frac{3\pi}{2}]\}$), and on the other hand, the intersection between the upper edge chain of $\cup_{\mathcal{Z}_i^k \in \Omega_2} \mathcal{Z}_i^k$ with the lower edge chain of $\cup_{\mathcal{Z}_i^k \in \Omega_1} \mathcal{Z}_i^k$ (which both belong to $\{(u,\theta) \in S^1 \times S^1 \mid \theta \in [u - \frac{\pi}{2}, u + \frac{\pi}{2}]\}$). These intersections can simply be performed by following the two edge chains for u from 0 to 2π, since they are monotone in u by Lemma 4.3.

Let us analyze the complexity of the above construction. The k_{i_0} helicoidal vol-

umes $\mathcal{H}_i$ that intersect $\mathcal{C}_{i_0}$ can be found in $O(k_{i_0})$ amortized time once the Delaunay triangulation of the footholds has been computed, which can be done in $O(n \log n)$ time [5, 17]. By Proposition 4.9, the upper and lower envelopes can be computed in $O(k_{i_0} \log k_{i_0})$ time using $O(k_{i_0} \alpha(k_{i_0}))$ space where α is the pseudo inverse of the Ackerman's function [6]. Also by Proposition 4.9, the union of Ω_1 and Ω_2 can be done in linear time in the size of the edge chains, that is $O(k_{i_0} \alpha(k_{i_0}))$ time. Thus, we can compute $\cup_i \mathcal{Z}_i$ in $O(k_{i_0} \log k_{i_0})$ time using $O(k_{i_0} \alpha(k_{i_0}))$ space after $O(n \log n)$ preprocessing time. We can compute $\cup_{i \neq i_0} \mathcal{Z}_i$ similarly by removing $\mathcal{Z}^1_{i_0}$ and $\mathcal{Z}^2_{i_0}$ from Ω_2.

The contribution of C_{i_0} to $\partial(\mathcal{F})$ is, according to Proposition 4.1, $C_{i_0} \cap \partial(\mathcal{F}) = compl(p_{//\theta}(compl(\cup_i \mathcal{Z}_i))) \setminus int(compl(p_{//\theta}(compl(\cup_{i \neq i_0} \mathcal{Z}_i))))$. By Remark 3.7, $compl(p_{//\theta}(compl(\cup_i \mathcal{Z}_i)))$ and $compl(p_{//\theta}(compl(\cup_{i \neq i_0} \mathcal{Z}_i)))$ are the projections onto C_{i_0} of the largest vertical strips Σ_{i_0} and Σ'_{i_0} included in $\cup_i \mathcal{Z}_i$ and $\cup_{i \neq i_0} \mathcal{Z}_i$, respectively (see Figure 4.2). These projections are easily computed because the edges of $\cup_i \mathcal{Z}_i$ and $\cup_{i \neq i_0} \mathcal{Z}_i$ are monotone with respect to u (Lemma 4.3). These projections, and therefore the computation of $C_{i_0} \cap \partial(\mathcal{F})$, can thus be done in linear time and space in the size of $\cup_i \mathcal{Z}_i$ and $\cup_{i \neq i_0} \mathcal{Z}_i$, that is $O(k_{i_0} \alpha(k_{i_0}))$.

Moreover, we label an arc of $\partial(\mathcal{F})$ either by i if the arc belongs to the circle C_i or by (i, j) if the arc belongs to the straight line segment $[s_i, s_j]$. The labels of the edges of $\partial(\mathcal{F})$ incident to C_{i_0} can be found as follows, without increasing the complexity. An arc of $\partial(\mathcal{F}) \cap C_{i_0}$ corresponds to a vertical strip $\Sigma_{i_0} \setminus \Sigma'_{i_0}$. An endpoint P of such an arc is the projection of a vertical edge, or the projection of a point of intersection between two curved edges. In the first case, P is the intersection of C_{i_0} with some C_i and in the second case, P is the intersection of C_{i_0} with some line segment $[s_i, s_j]$. By the general position assumption, among the circles $C_1, \ldots, C_n$ and the line segments joining two footholds, the intersection between three circles or, two circles and a line segment or, one circle and two line segments, is empty. Thus, P is the intersection between C_{i_0} and either a unique C_i or a unique line segment $[s_i, s_j]$. Therefore, the edge of $\partial(\mathcal{F})$ incident to C_{i_0} at P is either a circular arc supported by C_i or a line segment supported by $[s_i, s_j]$. Hence, the labels of the edges of $\partial(\mathcal{F})$ incident to C_{i_0} can be found at no extra-cost during the construction.

Since $\mathcal{A}$ is the arrangement of the circles of radius R centered at the footholds, $\sum_{i_0=1}^{n} k_{i_0} = O(|\mathcal{A}|)$. The above considerations yield the following theorem:

THEOREM 4.10. *We can compute $\partial(\mathcal{F}) \cap \mathcal{A}$ and the labels of the edges of $\partial(\mathcal{F})$ incident to the arcs of $\partial(\mathcal{F}) \cap \mathcal{A}$ in $O(|\mathcal{A}| \log n)$ time using $O(|\mathcal{A}| \alpha(n))$ space.*

4.4. Computation of the arcs of $\partial(\mathcal{F})$ issued from a foothold. The previous section has shown how to compute all the vertices of $\mathcal{F}$ that are incident to at least one circular arc. It remains to find the vertices of $\mathcal{F}$ incident to two straight edges. As we have seen in Section 2, a vertex of $\mathcal{F}$ incident to two straight edges of $\partial(\mathcal{F})$ is a foothold. Furthermore, considering a foothold s_{i_0} in a cell Γ of $\mathcal{A}$, s_{i_0} is a vertex of $\mathcal{F}$ incident to two straight edges of $\partial(\mathcal{F})$ if and only if s_{i_0} is a vertex of the convex hull of the footholds reachable from s_{i_0}. The k'_{i_0} footholds contained in the disk of radius R centered at s_{i_0} can be found in $O(k'_{i_0})$ amortized time because we have already computed the Delaunay triangulation of the footholds [5, 17]. Thus, we can decide if s_{i_0} is a vertex of the convex hull of these k'_{i_0} footholds in $O(k'_{i_0})$ time and space. When s_{i_0} is a vertex of the convex hull, we can also find the two edges of the convex hull adjacent to s_{i_0} in $O(k'_{i_0})$ time and space. As the sum of the k'_i for $i \in \{1, \ldots, n\}$ is bounded by the size of $\mathcal{A}$, we obtain the following theorem:

THEOREM 4.11. *The footholds belonging to $\partial(\mathcal{F})$ and the labels of the arcs of $\partial(\mathcal{F})$ issued from these footholds can be found in $O(|\mathcal{A}|)$ time and space.*

4.5. Construction of $\mathcal{F}$.

THEOREM 4.12. *The free space of the spider robot can be computed in $O(|\mathcal{A}|\log n)$ time using $O(|\mathcal{A}|\alpha(n))$ space.*

Proof. By Theorem 4.10, we have computed all the circular arcs of $\partial(\mathcal{F})$ and the labels of the edges of $\partial(\mathcal{F})$ incident to them. By Theorem 4.11, we have computed all the vertices of $\partial(\mathcal{F})$ that are incident to two straight edges of $\partial(\mathcal{F})$ and the label of these two edges. It remains to sort the vertices of $\partial(\mathcal{F})$ that appear on the line segments $[s_i, s_j]$. We only consider the line segments $[s_i, s_j]$ such that the corresponding label (i, j) appears during previous computations. Then, we sort the vertices of $\partial(\mathcal{F})$ that belong to each such relevant line. Since $|\partial(\mathcal{F})| = \Theta(|\mathcal{A}|)$ [1], sorting all these vertices can be done in $O(|\mathcal{A}|\log n)$ time. A complete description of $\partial(\mathcal{F})$ then follows easily. □

5. Generalization to polygonal foothold regions.

5.1. Introduction and preliminaries. We consider now the case where the set of footholds is no longer a set of points but a set $\mathcal{S}$ of pairwise disjoint polygonal regions bounded by n line segments $e_1, \ldots, e_n$. Clearly, $\mathcal{S}$ is a subset of the free space $\mathcal{F}$ of the spider robot. Let $\mathcal{F}_e$ denote the free space of the spider robot using as foothold regions only the edges $e_1, \ldots, e_n$. Suppose that the spider robot admits a stable placement outside $\mathcal{S}$ with its feet inside some polygonal footholds; then the placement remains stable if it retracts its legs on the boundary of these polygonal regions. Hence, $\mathcal{F} = \mathcal{F}_e \cup \mathcal{S}$. We show how to compute $\mathcal{F}_e$.

As observed in Remark 3.8, the results of Section 3 remains true if the foothold regions are line segments provided that $\mathcal{H}_i$ is replaced by $\mathcal{H}_{e_i}$ the generalized helicoidal volume defined by (see Figure 5.1):

$$\mathcal{H}_{e_i} = \{(P, \theta) \in I\!R^2 \times S^1 \mid P \in HD(s, \theta),\ s \in e_i\}.$$

The helicoidal volume associated to a point site s_i will be, henceforth, denoted by $\mathcal{H}_{s_i}$.

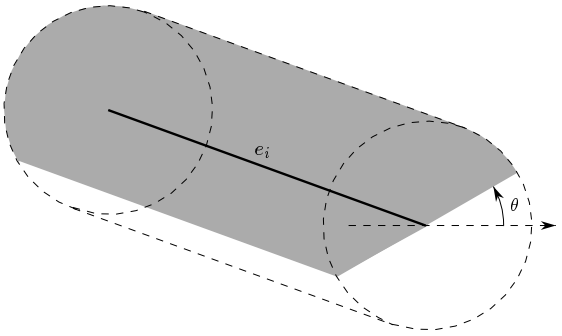

FIG. 5.1. *Section of $\mathcal{H}_{e_i}$ by the "plane" Π_θ.*

Similarly, we define the generalized circle C_{e_i} as the set of points at distance R from e_i. Let $\mathcal{A}_e$ denote the arrangement of the n generalized circles $C_{e_1}, \ldots, C_{e_n}$. Notice that $|\mathcal{A}_e| = \Theta(n^2)$.

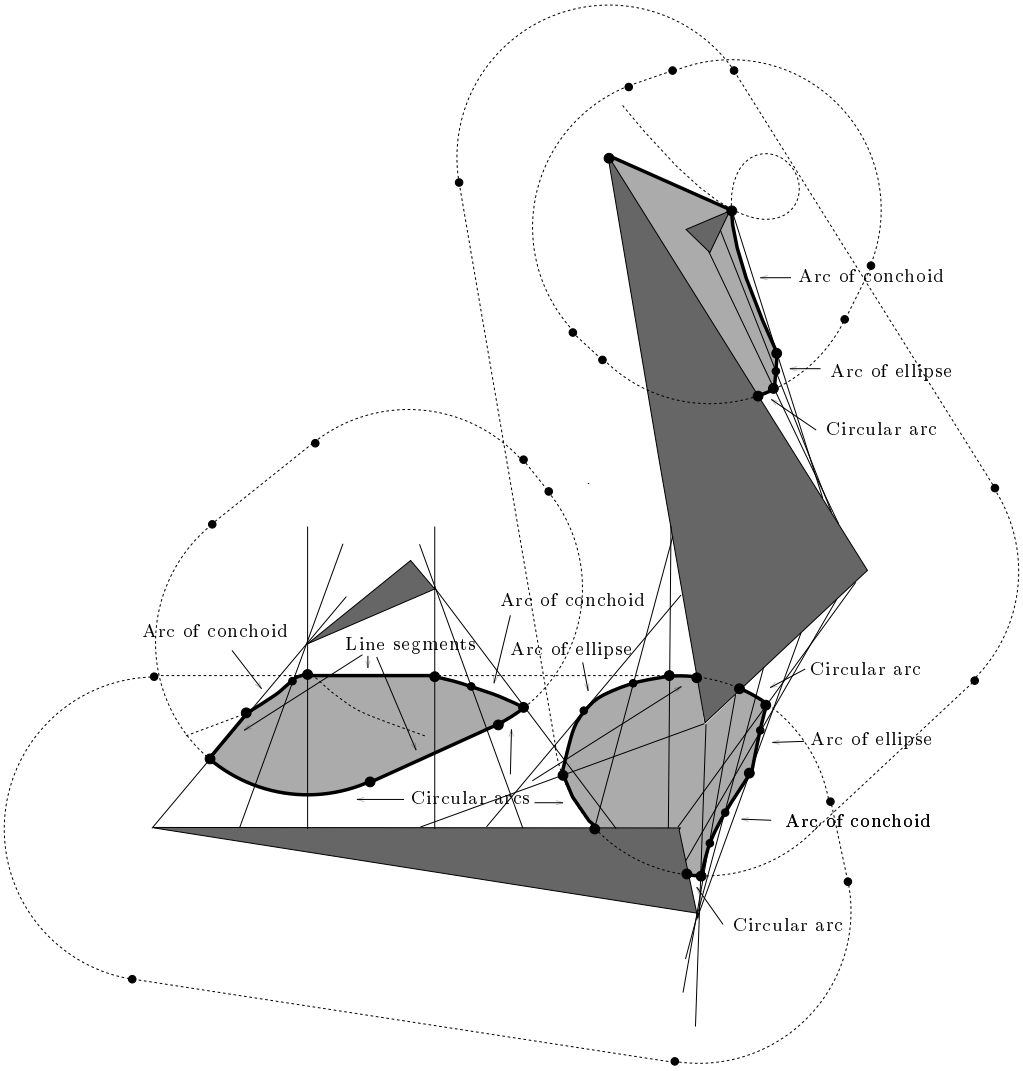

FIG. 5.2. *Example of free space $\mathcal{F}_e$ for polygonal foothold regions. The polygonal foothold regions are shown in dark grey. The other parts of $\mathcal{F}_e$ are in light grey. The C_{e_i} and some arcs of conchoid are dashed. All the line segments touching the polygons in two points are of length $2R$ and represent the ladder introduced in Section 5.3.*

Each arc of the boundary $\partial(\mathcal{F}_e)$ of $\mathcal{F}_e$ is either an arc of C_{e_i} corresponding to a maximal extension of one leg, or an arc corresponding to placements at the limit of stability of the spider robot. Similarly to what we did in Section 4, we compute first the contribution of each C_{e_i} to $\partial(\mathcal{F}_e)$ (Sections 5.2). Thereafter, we compute the arcs of $\partial(\mathcal{F}_e)$ that correspond to placements where the spider robot is at the limit of stability (Section 5.3). Finally, we show how to construct $\mathcal{F}_e$ (and $\mathcal{F}$) in Section 5.4.

Figure 5.2 shows an example of free space $\mathcal{F}_e$ for polygonal foothold regions.

5.2. Computation of $\partial(\mathcal{F}_e) \cap \mathcal{A}_e$. We compute the contribution to $\partial(\mathcal{F}_e)$ of each generalized circle C_{e_i} in turn. We consider the contribution of $C_{e_{i_0}}$ to $\partial(\mathcal{F}_e)$

for some $i_0 \in \{1, \ldots, n\}$. $C_{e_{i_0}}$ is composed of two half-circles and two straight line segments. In order to compute the contribution of $C_{e_{i_0}}$ to $\partial(\mathcal{F}_e)$, we evaluate first the contribution of the half-circles and then the contribution of the straight line segments. For convenience, we will not compute the contribution of the half-circles to $\partial(\mathcal{F}_e)$ but the contribution of the whole circles. Similarly, we will compute the contribution of the whole straight lines supporting the line segments of $C_{e_{i_0}}$.

Let s_{i_0} and s'_{i_0} denote the two endpoints of the line segment e_{i_0}, and let $C_{s_{i_0}}$ and $C_{s'_{i_0}}$ denote the unit circles centered at s_{i_0} and s'_{i_0} respectively. Let l_{i_0} and l'_{i_0} denote the two straight line segments of $C_{e_{i_0}}$, and L_{i_0} and L'_{i_0} their supporting lines. We show how to compute the contributions of $C_{s_{i_0}}$ and L_{i_0} to $\partial(\mathcal{F}_e)$; the contributions of $C_{s'_{i_0}}$ and L'_{i_0} can be computed likewise.

Let $\mathcal{C}_{s_{i_0}} = C_{s_{i_0}} \times S^1$ and $\mathcal{L}_{i_0} = L_{i_0} \times S^1$. Basically, we compute $\partial(\mathcal{F}_e) \cap C_{s_{i_0}}$ and $\partial(\mathcal{F}_e) \cap L_{i_0}$, as explained in Section 4.1, by computing $\cup_i(\mathcal{H}_{e_i} \cap \mathcal{C}_{s_{i_0}})$, $\cup_{i \neq i_0}(\mathcal{H}_{e_i} \cap \mathcal{C}_{s_{i_0}})$, $\cup_i(\mathcal{H}_{e_i} \cap \mathcal{L}_{i_0})$ and $\cup_{i \neq i_0}(\mathcal{H}_{e_i} \cap \mathcal{L}_{i_0})$. The properties of the new regions $\mathcal{Z}_{e_i} = \mathcal{H}_{e_i} \cap \mathcal{C}_{s_{i_0}}$ and $\mathcal{Y}_{e_i} = \mathcal{H}_{e_i} \cap \mathcal{L}_{i_0}$ are different though similar to the properties of $\mathcal{Z}_{s_i} = \mathcal{H}_{s_i} \cap \mathcal{C}_{s_{i_0}}$ described in Section 4.2. The analysis of $\mathcal{Z}_{e_i}$ and $\mathcal{Y}_{e_i}$ are subdivided into two parts: first, we consider the line D_i supporting e_i and we examine the regions $\mathcal{Z}_{D_i} = \mathcal{H}_{D_i} \cap \mathcal{C}_{s_{i_0}}$ and $\mathcal{Y}_{D_i} = \mathcal{H}_{D_i} \cap \mathcal{L}_{i_0}$ where $\mathcal{H}_{D_i}$ is the generalized helicoidal volume induced by D_i:

$$\mathcal{H}_{D_i} = \{(P, \theta) \in \mathbb{R}^2 \times S^1 \mid P \in HD(s, \theta),\ s \in D_i\}.$$

Then we deduce $\mathcal{Z}_{e_i}$ (resp. $\mathcal{Y}_{e_i}$) from $\mathcal{Z}_{D_i}$, $\mathcal{Z}_{s_i}$ and $\mathcal{Z}_{s'_i}$ (resp. $\mathcal{Y}_{D_i}$, $\mathcal{Y}_{s_i} = \mathcal{H}_{s_i} \cap \mathcal{L}_{i_0}$ and $\mathcal{Y}_{s'_i}$) where s_i and s'_i are the two endpoints of e_i. Thereafter, we compute the contribution of $C_{e_{i_0}}$ to $\partial(\mathcal{F}_e)$ in a way similar to what we did in Section 4.3. The following theorem sums up these results:

THEOREM 5.1. *We can compute $\partial(\mathcal{F}_e) \cap \mathcal{A}_e$ and the labels of the edges of $\partial(\mathcal{F}_e)$ incident to the arcs of $\partial(\mathcal{F}_e) \cap \mathcal{A}_e$ in $O(|\mathcal{A}_e| \alpha_7(n) \log n)$ time using $O(|\mathcal{A}_e| \alpha_8(n))$ space.* The proof of this theorem, omitted here, is a direct generalization of the proof of Theorem 4.10. Details are given in [4] or [12].

5.3. Arcs of $\partial(\mathcal{F}_e)$ corresponding to the placements where the spider robot is at the limit of stability. We now have to compute the edges of $\mathcal{F}_e$ that do not belong to $\mathcal{A}_e$. The arcs of $\partial(\mathcal{F}_e) \cap \mathcal{A}_e$ correspond to placements at the limit of accessibility of the spider robot, and vice versa. Thus, other edges of $\mathcal{F}_e$ correspond to placements at the limit of stability of the spider robot. We denote by $\partial(\mathcal{F}_e)_{stab}$ the set of those edges. A placement P of the spider robot is at the limit of stability if and only if there exists a closed half-disk of radius R centered at P that does not contain any foothold except at least two footholds located on the diameter of the half-disk such that P is between these footholds (see Figure 5.3). Therefore, the edges of $\partial(\mathcal{F}_e)_{stab}$ are portions of the curves drawn by the midpoint of a ladder of length $2R$ moving by translation and rotation such that the ladder touches the boundary of the foothold regions in two points but does not intersect the interior of the foothold regions. Hence, the edges of $\partial(\mathcal{F}_e)_{stab}$ are supported by the projection (onto $\mathbb{R}^2$) of the edges of the boundary of the free space of the ladder moving by translation and rotation amidst the foothold regions considered as obstacles, i.e., the set of $(P, \theta) \in \mathbb{R}^2 \times \mathbb{R}/\pi\mathbb{Z}$ such that the ladder of length $2R$ that has its midpoint at P and makes an angle θ with the x-axis does not properly intersect the interior of the foothold regions. According to [16], the edges of the boundary of the free space of the ladder can be computed in $O(|\mathcal{A}_e| \log n)$ time using $O(|\mathcal{A}_e|)$ space. The projection (onto $\mathbb{R}^2$) of each edge can

easily be computed in constant time. Thus, we can compute, in $O(|\mathcal{A}_e| \log n)$ time and $O(|\mathcal{A}_e|)$ space (using [16]), a set of curves in $\mathbb{R}^2$ that contains the arcs of $\partial(\mathcal{F}_e)$ that correspond to placements at the limit of stability of the spider robot. However, it remains to compute the portions of these curves that belong to $\partial(\mathcal{F}_e)$.

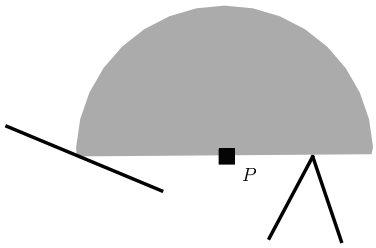

FIG. 5.3. *Example of placement P at the limit of stability.*

5.3.1. Notations and definitions. The relative interior of an e_i is called a *wall*. An endpoint of an e_i is called a *corner* (when several walls share an endpoint, we define only one corner at that point). The *ladder* is a line segment of length $2R$. A *placement* of the ladder is a pair $(P, \theta) \in \mathbb{R}^2 \times \mathbb{R}/\pi\mathbb{Z}$ where P is the location of the midpoint of the ladder and θ is the angle between the x-axis and the ladder. A *free placement* of the ladder is a placement where the ladder does not properly intersect the walls or partially lies on some walls and does not properly intersect the others (if none of the polygonal regions of $\mathcal{S}$ are degenerated into line segments or points, then a free placement of the ladder is a placement where the ladder does not intersect the interior of the polygonal regions of $\mathcal{S}$). A *placement of type corner-ladder* is a placement of the ladder such that the relative interior of the ladder touches a *corner*. A *placement of type wall-endpoint* is a placement of the ladder such that an endpoint of the ladder touches a *wall*. A *placement of type corner-endpoint* is a placement of the ladder such that an endpoint of the ladder touches a corner. We now define *k-contact placements* of the ladder.

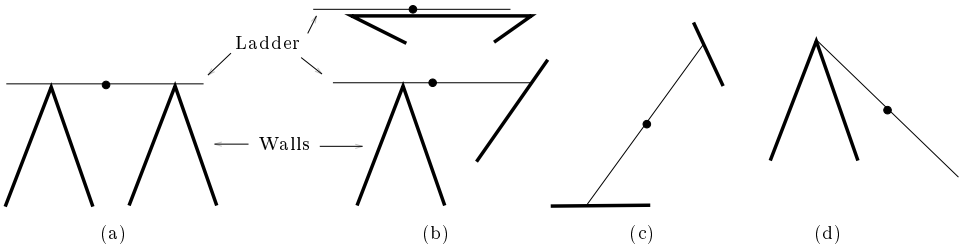

FIG. 5.4. *Examples of 2-contact placements of type (a): (corner-ladder)^2, (b): (corner-ladder, wall-endpoint), (c): (wall-endpoint)^2 and (d): (corner-endpoint).*

A *1-contact placement* is a free placement of type corner-ladder or wall-endpoint. A *2-contact placement* is either the combination of two 1-contact placements or a free placement of type corner-endpoint. A 2-contact placement is said to be of type (corner-ladder)^2, (corner-ladder, wall-endpoint), (wall-endpoint)^2, or (corner-endpoint), in accordance to the types of placements involved in the 2-contact placement (see Figure 5.4). Given two walls (resp. a wall and a corner, two corners, one corner), the set of 2-contact placements induced by these two walls (resp. the wall

and the corner, the two corners, the single corner) is called a *2-contact curve*. The type of a 2-contact curve is the type of the 2-contact placement defining the curve. Note that the 2-contact curves are defined in $\mathbb{R}^2 \times \mathbb{R}/\pi\mathbb{Z}$. A *3-contact placement* is a combination of a 1-contact placement and a 2-contact placement. The types of 3-contact placements are naturally given by (corner-ladder)^3, (corner-endpoint, wall-endpoint)... With this definition, we unfortunately cannot guarantee that all the 2-contact curves end at 3-contact placements. Indeed, a 2-contact curve defined by the ladder sliding along a wall (see Figure 5.4b) ends on one side (if no other wall blocks the sliding motion) at a 2-contact placement of type (corner-endpoint), where the ladder is collinear with the wall, without properly intersecting it. In order to ensure that all the 2-contact curves end at 3-contact placements, we consider these 2-contact placements as 3-contact placements, and denote their type by (corner-endpoint, $\|$). A *k-contact placement*, $k > 3$, is the combination of p 1-contact placements, q 2-contact placements and r 3-contact placements such that $p + 2q + 3r = k$.

Now, we define a *2-contact tracing* as the projection onto $\mathbb{R}^2$ of a 2-contact curve. Similarly as above, we define the types of the 2-contact tracings. Notice that, to any point P on a given 2-contact tracing $\mathcal{K}$, corresponds a unique placement (P, θ) on the 2-contact curve that projects onto $\mathcal{K}$. It follows that, to any point P on a 2-contact tracing $\mathcal{K}$, corresponds a unique pair (M, N) of points of contact between the ladder at (P, θ) and the walls (M and N are equal when $\mathcal{K}$ is a 2-contact tracing of type (corner-endpoint)); when P is an endpoint of $\mathcal{K}$, a 3-contact placement corresponds to P, however, (M, N) is uniquely defined by continuity. The points M and N are called the *contact points corresponding to* $P \in \mathcal{K}$. We also define the three contact points corresponding to a 3-contact placement.

A 2-contact tracing is either a straight line segment, an arc of ellipse, an arc of conchoid or a circular arc. Indeed (see Figures 5.5, 5.6, 5.7 and 5.8), a 2-contact tracing of type (corner-endpoint) is a circular arc; a 2-contact tracing of type (wall-endpoint)^2 is an arc of ellipse; a 2-contact tracing of type (corner-ladder, wall-endpoint) is an arc of conchoid (see [4]); a 2-contact tracing of type (corner-ladder)^2 is a straight line segment. As we said before, we can compute all these 2-contact tracings in $O(|\mathcal{A}_e| \log n)$ time using $O(|\mathcal{A}_e|)$ space [16], and it remains to compute the portions of these curves that belong to $\partial(\mathcal{F}_e)$.

5.3.2. Overview. We first show that only some portions of the 2-contact tracings correspond to positions at the limit of stability of the spider robot (Section 5.3.3). These portions are called the relevant 2-contact tracings. Then, we prove that we do not have to take into consideration the intersections between the relative interior of relevant 2-contact tracings (Proposition 5.2). We also show that, if a point A is an endpoint of several relevant 2-contact tracings, only two of them can support edges of $\partial(\mathcal{F}_e)_{stab}$ in the neighborhood of A (Propositions 5.3). Finally (Section 5.3.4), we compute a graph whose edges are relevant 2-contact tracings and where the degree of each node is at most two. This graph induces a set Δ of curves supporting $\partial(\mathcal{F}_e)_{stab}$ (Theorem 5.4) that will allow us to compute $\partial(\mathcal{F}_e)_{stab}$ in Section 5.4.

5.3.3. Relevant 2-contact tracings. As mentioned above, a placement P of the spider robot is at the limit of stability if and only if there exists a closed half-disk of radius R centered at P that does not contain any foothold except at least two footholds located on the diameter of the half-disk, one on each side of P. Thus, a point P of a 2-contact tracing $\mathcal{K}$ belongs to an arc of $\partial(\mathcal{F}_e)_{stab}$ only if P lies between the two contact points corresponding to $P \in \mathcal{K}$. The portions of the 2-contact tracings for which that property holds are called the *relevant 2-contact tracings*. The other

portions are called the *irrelevant 2-contact tracings*. We now show how to compute the relevant 2-contact tracings for each type of contact. Let $\mathcal{K}$ denote a 2-contact tracing, let $P \in \mathcal{K}$ and let M and N be the two contact points corresponding to $P \in \mathcal{K}$. In Figures 5.5, 5.6, 5.7 and 5.8, the walls and the relevant 2-contact tracings are thick, the irrelevant 2-contact tracings are dashed thick, and the ladder is thin.

Type (corner-endpoint):
$\mathcal{K}$ is a circular arc, M and N coincide with one endpoint of the ladder. Thus, all the 2-contact tracings of type (corner-endpoint) are wholly irrelevant.

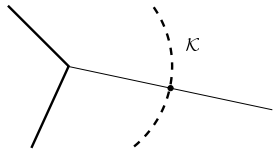

FIG. 5.5. *Irrelevant 2-contact tracing of type (corner-endpoint), i.e., circular arc.*

Type (wall-endpoint)^2:
$\mathcal{K}$ is an arc of ellipse, M and N are the endpoints of the ladder and thus, P lies between them. Therefore, all the 2-contact tracings of type (wall-endpoint)^2 are wholly relevant.

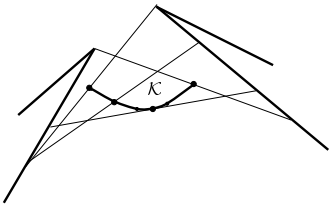

FIG. 5.6. *Relevant 2-contact tracing of type (wall-endpoint)^2, i.e., arc of ellipse.*

Type (corner-ladder, wall-endpoint):

$\mathcal{K}$ is an arc of conchoid. If the distance between the corner and the wall is greater than R, then $\mathcal{K}$ is wholly relevant.

Otherwise, if that distance is smaller than R, then, the two relevant portions and the irrelevant portion of $\mathcal{K}$ are incident to the corner involved in the type of $\mathcal{K}$.

Notice that, if the corner is an endpoint of the wall (see Figure 5.4b), then $\mathcal{K}$ degenerates into a line segment and the irrelevant portion of $\mathcal{K}$ is the portion which is not supported by the wall.

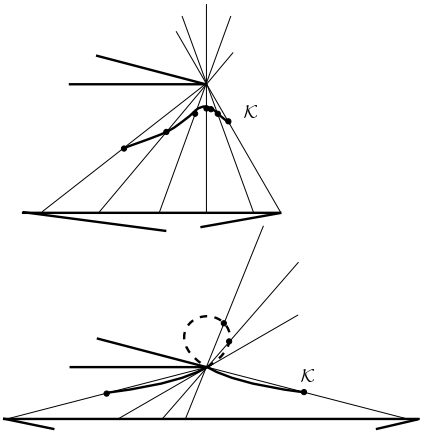

FIG. 5.7. *Relevant, and partially relevant, 2-contact tracings of type (corner-ladder, wall-endpoint), i.e., arcs of conchoid.*

Type (corner-ladder)^2:
$\mathcal{K}$ is a line segment. If the distance between the two corners is greater than R, then $\mathcal{K}$ is wholly relevant; otherwise, the portion of $\mathcal{K}$ which is relevant, is the line segment joining the two corners.

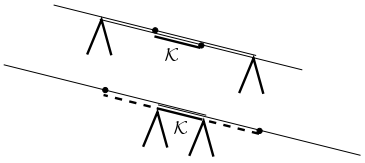

FIG. 5.8. *Relevant, and partially relevant, 2-contact tracings of type (corner-ladder)^2.*

We now show that the intersections between the relative interiors of the relevant 2-contact tracings are not interesting for the spider robot motion problem. We recall that, if a vertex A of $\partial(\mathcal{F}_e)$ belongs to $\mathcal{A}_e$, then we know by Theorem 5.1 the labels of the edges of $\partial(\mathcal{F}_e)$ incident to A. Otherwise, if $A \notin \mathcal{A}_e$, then the two edges of $\partial(\mathcal{F}_e)$ that end at A correspond to placements at the limit of stability of the spider robot.

PROPOSITION 5.2. *Any vertex A of $\partial(\mathcal{F}_e)$, such that $A \notin \mathcal{A}_e$, is an endpoint of the two relevant 2-contact tracings supporting the edges of $\partial(\mathcal{F}_e)$ ending at A.*

Proof. Since the two edges of $\partial(\mathcal{F}_e)$ that end at A correspond to placements at the limit of stability of the spider robot, they are both supported by some relevant 2-contact tracings. Thus, we only have to prove that A is an endpoint of these two relevant 2-contact tracings.

Let $\mathcal{K}_1$ and $\mathcal{K}_2$ be these two relevant 2-contact tracings and assume for a contradiction that A is not an endpoint of $\mathcal{K}_1$ (nothing is assumed for A with respect to $\mathcal{K}_2$). Let $L_1 = (A, \theta_1)$ (resp. $L_2 = (A, \theta_2)$) be the placement of the ladder that correspond to $A \in \mathcal{K}_1$ (resp. $A \in \mathcal{K}_2$) and let M_1 and N_1 (resp. M_2 and N_2) be the corresponding contact points (see Figure 5.9). First, notice that $L_1 \neq L_2$. Indeed, otherwise, L_1 is at least a 3-contact placement and then, A must be an endpoint of $\mathcal{K}_1$, which contradicts our assumption.

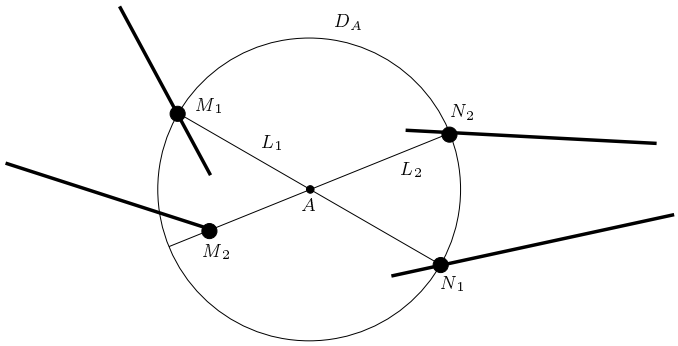

FIG. 5.9. *For the proof of Proposition 5.2.*

By the definition of the relevant 2-contact tracings, A is between M_1 and N_1. Moreover, A cannot be equal to M_1 or N_1 since A is not an endpoint of $\mathcal{K}_1$. It follows that neither M_2 nor N_2 is equal to A, because otherwise L_1 would be a 3-contact placement. Therefore, A is strictly between M_1 and N_1, and strictly between M_2 and N_2. Thus, A is strictly inside the polygon $(M_1M_2N_1N_2)$.

On the other hand, since $A \notin \mathcal{A}_e$, A does not belong to any C_{e_i}, and therefore, the walls supporting M_1, N_1, M_2 and N_2 intersect the open disk D_A of radius R centered at A. Thus, there exists four points M_1', N_1', M_2' and N_2' on these walls and in D_A, that are close enough to M_1, N_1, M_2 and N_2 respectively to ensure that A belongs to the interior of the polygon $(M_1'M_2'N_1'N_2')$. Since the distances from A to M_1', N_1', M_1' and N_2', are strictly smaller than R, A belongs to the interior of $\mathcal{F}_e$. This contradicts our assumption that A is a vertex of $\partial(\mathcal{F}_e)$ and yields the result. □

Consider now the adjacency graph $\mathcal{G}$ of the relevant 2-contact tracings such that two relevant 2-contact tracings are connected in $\mathcal{G}$ if and only if they have a common endpoint (the intersections between the relative interiors of the relevant 2-contact tracings are not considered). Notice that, given the set of relevant 2-contact tracings, $\mathcal{G}$ can be easily computed in $O(|\mathcal{A}_e| \log n)$ time. Now, given two vertices of $\partial(\mathcal{F}_e) \cap \mathcal{A}_e$

that are connected along $\partial(\mathcal{F}_e)$ by arcs of $\partial(\mathcal{F}_e)_{stab}$, we want to compute these arcs. For computing these arcs, we cannot simply use the graph $\mathcal{G}$ because the degree of some nodes of $\mathcal{G}$ may be arbitrarily large (see Figure 5.10). We show in the next proposition that we can deduce from $\mathcal{G}$ a graph $\mathcal{G}^*$ such that the degree of each node of $\mathcal{G}^*$ is at most two and that $\mathcal{G}^*$ supports any portion of $\partial(\mathcal{F}_e)$ which is the concatenation of arcs of $\partial(\mathcal{F}_e)_{stab}$.

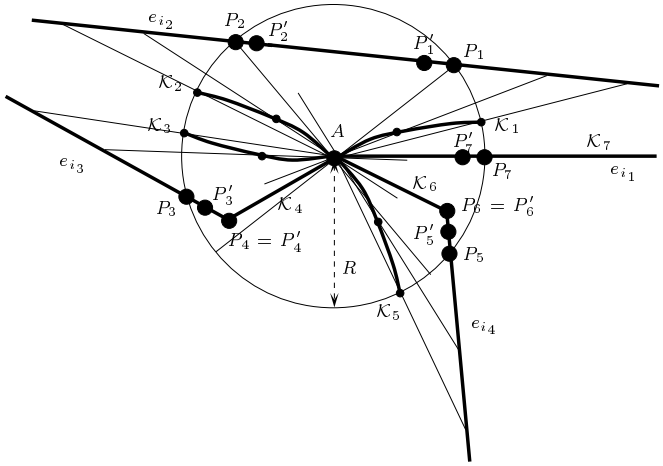

FIG. 5.10. *Relevant 2-contact tracings $\mathcal{K}_1, \ldots, \mathcal{K}_7$ ending at A. $\mathcal{K}_1, \mathcal{K}_2, \mathcal{K}_3$ and $\mathcal{K}_5$ are 2-contact tracings of type (corner-ladder, wall-endpoint) (i.e., arcs of conchoid). $\mathcal{K}_7$ is a degenerated 2-contact tracing of type (corner-ladder, wall-endpoint) (i.e., a line segment). $\mathcal{K}_4$ and $\mathcal{K}_5$ are 2-contact tracings of type (corner-ladder)^2 (i.e., line segments).*

We consider four hypotheses (H1,...,H4) that obviate the need to consider degenerate cases. They are not essential but substantially simplify the proof of the following proposition. The first three hypotheses are made to ensure that the degree of each vertex of the free space of the ladder is three.

H1 The line segments $e_1, \ldots, e_n$ compose the boundary of a set of non degenerated polygons (i.e., no polygon is reduced to a line segment or to a point).

H2 The ladder does not admit any 4-contact placement.

H3 The arc (of conchoid) drawn by an endpoint of the ladder when its other endpoint moves along a wall while the ladder remains in contact with a corner, is not tangent to any other wall.

H4 The ladder does not admit any 3-contact placement when its midpoint is located at a corner.

PROPOSITION 5.3. *For any node A of $\mathcal{G}$ of degree k such that $A \notin \mathcal{A}_e$, at most two relevant 2-contact tracings can support $\partial(\mathcal{F}_e)$ in a sufficiently small neighborhood of A. Moreover, we can determine these at most two curves in $O(k \log k)$ time using $O(k)$ space.*

Proof. Let $A \notin \mathcal{A}_e$ be a node of $\mathcal{G}$ of degree k. We assume that $k > 2$, otherwise Proposition 5.3 is trivial. Let $\mathcal{K}_1, \ldots, \mathcal{K}_k$ be the relevant 2-contact tracings that end at A, and let $L_i = (A, \phi_i)$ be the placement of the ladder that corresponds to $A \in \mathcal{K}_i$. D_A is the open disk of radius R centered at A. We distinguish two cases whether A is a corner or not.

Case 1: A is a corner. (See Figure 5.10.)

The 2-contact tracing $\mathcal{K}_i$ involves at least another contact than the corner-ladder

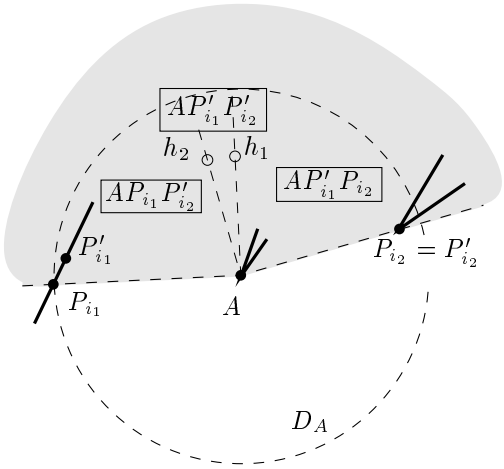

FIG. 5.11. *Wedge $P_{i_1}AP_{i_2}$ is in $\mathcal{F}_e$ near A.*

contact at A. This contact cannot be of type corner-endpoint by Hypothesis H4. If the contact is of type wall-endpoint, we define P_i as the contact point between this wall and the ladder at placement L_i (see Figure 5.11). Since $A \notin \mathcal{A}_e$, the wall must intersect D_A and we define P'_i as a point close to P_i in that intersection. If the contact is of type corner-ladder, we define $P_i = P'_i$ as the corner (distinct from A) involved in this contact (notice that $P_i = P'_i \in D_A$ by Hypothesis H4).

Fact: $\forall i \neq j, \ \ \phi_i \neq \phi_j$.
Otherwise, $L_i = L_j$ is a 3-contact placement contradicting Hypothesis H4.

Fact: *A is a non-flat vertex of CH$(A, P_1, \ldots, P_k)$ or belongs to the interior of $\mathcal{F}_e$.*
Assume that $A \in \partial(\mathcal{F}_e)$. Then, A lies on the boundary of CH$(A, P_1, \ldots, P_k)$ because, otherwise, the P'_i provide footholds such that the spider robot can move in a neighborhood of A. Furthermore, A must be a non-flat vertex of CH$(A, P_1, \ldots, P_k)$, by Hypothesis H4.

Assume now that $A \in \partial(\mathcal{F}_e)$, and let P_{i_1} and P_{i_2} be the two vertices of CH$(A, P_1, \ldots, P_k)$ such that P_{i_1}, A and P_{i_2} are consecutive along the boundary of CH$(A, P_1, \ldots, P_k)$ (see Figure 5.11). We will exhibit a stable placement for the spider robot at any position P inside the intersection of the wedge $P_{i_1}AP_{i_2}$ and a neighborhood of A. Let h_1 and h_2 be two points in the wedge $P_{i_1}AP_{i_2}$ such that the wedges $P_{i_1}Ah_1$ and $h_2AP_{i_2}$ are right (see Figure 5.11).
— If P is in the wedge $P_{i_1}Ah_2$, and is close enough to A, the footholds A, P_{i_1} and P'_{i_2} yield a stable placement for the spider robot.
— If P is in the wedge h_2Ah_1, and is close enough to A, footholds A, P'_{i_1} and P'_{i_2} yield a stable placement for the spider robot.
— If P is in the wedge $h_1AP_{i_1}$, and is close enough to A, footholds A, P'_{i_1} and P_{i_2} yields a stable placement for the spider robot.

Fact: *$\mathcal{K}_i$, $i \notin \{i_1, i_2\}$, cannot support an edge of $\partial(\mathcal{F}_e)$ incident to A.*
We assume that $A \in \partial(\mathcal{F}_e)$ because, otherwise, the claim is obvious. It follows that A is a non-flat vertex of CH$(A, P_1, \ldots, P_k)$. A 2-contact tracing $\mathcal{K}_i$, $i \notin \{i_1, i_2\}$, cannot be an arc of ellipse because, otherwise, L_i is a 3-contact placement (because A is here a corner) contradicting Hypothesis H4. Then, $\mathcal{K}_i$ can be either the segment AP_i or an arc of conchoid. If $\mathcal{K}_i$ is an arc of conchoid, then, by the general properties of

conchoids (see [4]), $\mathcal{K}_i$ is tangent to the segment AP_i at A. Thus, $\mathcal{K}_i$ is always tangent to the segment AP_i at A. The point P_i strictly belongs to the wedge $P_{i_1}AP_{i_2}$, because we have shown that $\phi_i \notin \{\phi_{i_1}, \phi_{i_2}\}$. Thus, in a neighborhood of A, $\mathcal{K}_i$ is strictly inside the wedge $P_{i_1}AP_{i_2}$ and thus strictly inside $\mathcal{F}_e$. Therefore, $\mathcal{K}_i$ cannot support $\partial(\mathcal{F}_e)$, in a neighborhood of A.

Hence, by sorting the P_i by their polar angles around A, we can determine, in $O(k \log k)$ time, if A is a non-flat vertex of $\mathrm{CH}(A, P_1, \ldots, P_k)$, and if so, determine i_1 and i_2. If A is a non-flat vertex of $\mathrm{CH}(A, P_1, \ldots, P_k)$, then, only $\mathcal{K}_{i_1}$ and $\mathcal{K}_{i_2}$ can support an edge of $\partial(\mathcal{F}_e)$ incident to A. Otherwise, A belongs to the interior of $\mathcal{F}_e$ and none of the 2-contact tracings $\mathcal{K}_1, \ldots, \mathcal{K}_k$ can support an edge of $\partial(\mathcal{F}_e)$ incident to A.

Case 2: A is not a corner.

Fact: *If there exists $i \neq j$ such that $\phi_i \neq \phi_j$, then A belongs to the interior of $\mathcal{F}_e$.*

For each relevant 2-contact placement $L_i = (A, \phi_i)$, there exists two contact points M_i and N_i on each side of A at distance less or equal to R. Since A is not a corner, neither M_i nor N_i is equal to A, thus A belongs to the relative interior of the segment M_iN_i. It follows, when $\phi_i \neq \phi_j$, that A belongs to the interior of the polygon $(M_iM_jN_iN_j)$ (see Figure 5.9). Similarly as in the proof of Proposition 5.2, since $A \notin \mathcal{A}_e$, there exists four footholds M_i', N_i', M_j', N_j' in D_A and in some neighborhoods of M_i, N_i, M_j, N_j, respectively, such that A belongs to the interior of the polygon $(M_i'M_j'N_i'N_j')$. Thus, A belongs to the interior of $\mathcal{F}_e$.

Hence, if there exists $i \neq j$ such that $\phi_i \neq \phi_j$, none of the 2-contact tracings $\mathcal{K}_1, \ldots, \mathcal{K}_k$ can support an edge of $\partial(\mathcal{F}_e)$ incident to A. We now assume that $\phi_i = \phi_j$, $\forall i, j$.

Fact: *There are at most six 2-contact tracings incident to A.*

The general position hypothesis H2 forbid k-contacts for $k > 3$, thus A corresponds to a 3-contact placement. The three possible choices of two contacts among three, give three 2-contact tracing intersecting in A and thus, six arcs incident to A.

Fact: *There are three 2-contact tracings incident to A.*

If the 3-contact placement L is of type (corner-endpoint, $\|$), then there are only three 2-contact tracings incident to A, that are two circular arcs and one line segment. Otherwise, it comes from the general position hypotheses H1, H2 and H3 (designed to ensure that property) that a 2-contact tracing cannot be valid on both side of the 3-contact, i.e., on one side of the 3-contact placement, the placements are not free. The proof that the hypotheses ensured that fact is detailed in [4].

Fact: *There are two relevant 2-contact tracings incident to A.*

Since A is not a corner, at the 3-contact placement L, two contact points are on the same side of A. Thus, only two of the three 2-contact tracings incident to A are relevant. □

5.3.4. Construction of Δ. Now, consider the graph $\mathcal{G}$ and each node A in turn. If $A \in \mathcal{A}_e$, we disconnect all the edges of $\mathcal{G}$ that end at A. Notice that for each such node A, we know, by Theorem 5.1, whether $A \in \partial(\mathcal{F}_e)$ and, in such a case, the labels of the edges of $\partial(\mathcal{F}_e)$ incident to A. If $A \notin \mathcal{A}_e$, we disconnect the edges ending at A except those (at most two) that may support $\partial(\mathcal{F}_e)$ in a neighborhood of A (see Proposition 5.3). In this way, we obtain a graph $\mathcal{G}^*$ such that the degree of each node is one or two. We consider each connected component of this new graph as a curve. Let Δ be this set of curves. These curves are represented in $\mathcal{G}^*$ as chains (open or closed). It follows that, even if a curve is not simple, there exists a natural order along

the curve. Then, according to Propositions 5.2 and 5.3, we get the following theorem:

THEOREM 5.4. *We can compute, in $O(|\mathcal{A}_e| \log n)$ time using $O(|\mathcal{A}_e|)$ space, a set Δ of curves that support the edges of $\partial(\mathcal{F}_e)$ corresponding to placements at the limit of stability of the spider robot. Moreover, any portion $\mathcal{P}$ of $\partial(\mathcal{F}_e)$ either intersects $\mathcal{A}_e$ or belongs to a unique curve of Δ.*

5.4. Construction of $\mathcal{F}_e$ and $\mathcal{F}$. We can now construct $\mathcal{F}_e$ and $\mathcal{F}$. Let $\lambda_k(n)$ denote the maximum length of the Davenport-Schinzel sequence of order k on n symbols and $\alpha_k(n) = \lambda_k(n)/n$. Note that $\alpha_3(n) = \alpha(n)$.

THEOREM 5.5. *Given, as foothold regions, a set of n non intersecting straight line segments that satisfies Hypotheses H1, H2, H3 and H4, we can compute the free space $\mathcal{F}_e$ of the spider robot in $O(|\mathcal{A}_e|\alpha_8(n) \log n)$ time using $O(|\mathcal{A}_e|\alpha_8(n))$ space.*

Proof. By Theorem 5.1, we can compute the contribution of $\mathcal{A}_e$ to $\partial(\mathcal{F}_e)$ and the label of the edges of $\partial(\mathcal{F}_e)$ incident to them in $O(|\mathcal{A}_e|\alpha_7(n) \log n)$ time using $O(|\mathcal{A}_e|\alpha_8(n))$ space. By Theorem 5.4, we can compute, in $O(|\mathcal{A}_e| \log n)$ time using $O(|\mathcal{A}_e|)$ space, a set Δ of curves that support the edges of $\partial(\mathcal{F}_e)$ that do not belong to $\mathcal{A}_e$. Moreover, any portion $\mathcal{P}$ of $\partial(\mathcal{F}_e)$ such that $\mathcal{P} \cap \mathcal{A}_e = \emptyset$ belongs to a unique curve of Δ. Thus, by sorting all the vertices of $\partial(\mathcal{F}_e) \cap \mathcal{A}_e \cap \Delta$ on the relevant curves of Δ, we obtain all the edges of $\partial(\mathcal{F}_e)$ that belong to a connected component of $\partial(\mathcal{F}_e)$ intersecting $\mathcal{A}_e$. Indeed, for each vertex $A \in \partial(\mathcal{F}_e) \cap \mathcal{A}_e \cap \Delta$, we know, in a neighborhood of A, the portion of the curve of Δ that belongs to $\partial(\mathcal{F}_e)$ because we can simply determine, for each edge, a side of the edge that belongs to $\mathcal{F}_e$ (the contact points corresponding to the edges determine a side that necessarily belongs to $\mathcal{F}_e$)[4]. Then, it is an easy task to deduce all the connected components of $\partial(\mathcal{F}_e)$ that intersect $\mathcal{A}_e$.

It remains to compute the connected components of $\partial(\mathcal{F}_e)$ that do not intersect $\mathcal{A}_e$. Each of these components must be a closed curve of Δ. Moreover, all the curves of Δ belong to $\mathcal{F}_e$. Thus, according to Theorem 5.4, any closed curve $\mathcal{K}$ of Δ that does not intersect $\mathcal{A}_e$ is either a connected component of $\partial(\mathcal{F}_e)$ or is strictly included in $\mathcal{F}_e$. Therefore, by considering, in addition, all the closed curves of Δ that do not intersect $\mathcal{A}_e$, we finally obtain a set Ψ of closed curves that contains $\partial(\mathcal{F}_e)$ and such that any curve of Ψ is either a connected component of $\partial(\mathcal{F}_e)$ or is strictly included in $\mathcal{F}_e$.

At last, as we can simply determine, for each curve of Ψ, a side of the edge that belongs to $\mathcal{F}_e$, we can easily deduce from Ψ the free space $\mathcal{F}_e$. That concludes the proof since all these computations can be done in $O(|\mathcal{A}_e|\alpha_8(n) \log n)$ time using $O(|\mathcal{A}_e|\alpha_8(n))$ space. □

As we said at the beginning of Section 5, the free space of the spider robot using as foothold regions a set of polygonal regions is obtained by adding these polygonal regions to $\mathcal{F}_e$. This does not increase the geometric complexity of the free space nor the complexity of the computation. Thus, we get the following theorem:

THEOREM 5.6. *Given a set of pairwise disjoint polygonal foothold regions with n edges in total that satisfies Hypotheses H1, H2, H3 and H4, we can compute the free space $\mathcal{F}$ of the spider robot in $O(|\mathcal{A}_e|\alpha_8(n) \log n)$ time using $O(|\mathcal{A}_e|\alpha_8(n))$ space.*

The function $\alpha_8(n)$ is extremely slowly growing and can be considered as a small constant in practical situations. This result is almost optimal since, as shown in [1], $\Omega(|\mathcal{A}_e|)$ is a lower bound for the size of $\mathcal{F}$.

[4] Observe that when the edge belongs to $\mathcal{F}_e$, its two sides belong to $\mathcal{F}_e$.

6. Conclusion. We have seen in Theorem 4.12 that, when the foothold regions are n points in the plane, the free space of the spider robot can be computed in $O(|\mathcal{A}| \log n)$ time using $O(|\mathcal{A}|\alpha(n))$ space where $\alpha(n)$ is the pseudo inverse of the Ackerman's function and $\mathcal{A}$ the arrangement of the n circles of radius R centered at the footholds. By [1] the size of $\mathcal{F}$ is known to be $\Theta(|\mathcal{A}|)$. The size of $\mathcal{A}$ is $O(n^2)$ but it has been shown in [15] that $|\mathcal{A}| = O(kn)$, where k denotes the maximum number of disks of radius R centered at the footholds that can cover a point of the plane. Thus, in case of sparse footholds, the sizes of $\mathcal{A}$ and $\mathcal{F}$ are linearly related to the number of footholds.

When the foothold regions are polygons with n edges in total, the free space of the spider robot can be computed in $O(|\mathcal{A}_e|\alpha_8(n) \log n)$ time using $O(|\mathcal{A}_e|\alpha_8(n))$ space, where $n\alpha_k(n) = \lambda_k(n)$ is the maximum length of a Davenport-Schinzel sequence of order k on n symbols, and $\mathcal{A}_e$ is the arrangement of the n curves consisting of the points lying at distance R from the straight line edges. Note that the size of $\mathcal{A}_e$ is $O(n^2)$.

It should be observed that, in the case of point footholds, our algorithm implies that $O(|\mathcal{A}|\alpha(n))$ is an upper bound for $|\mathcal{F}|$. However, this bound is not tight since $|\mathcal{F}| = \Theta(|\mathcal{A}|)$ [1]. In the case of polygonal footholds, our analysis implies that $O(|\mathcal{A}_e|\alpha_8(n))$ is an upper bound for $|\mathcal{F}|$. We leave as an open problem to close the (small) gap between this upper bound and the $\Omega(|\mathcal{A}_e|)$ lower bound.

Once the free space $\mathcal{F}$ is known, several questions can be answered. In particular, given two points in the same connected component of $\mathcal{F}$, the algorithm in [1] computes a motion of the spider robot, i.e., a motion of the body and a corresponding sequence of leg assignments that allows the robot to move from one point to the other.

The motion planning problem for other types of legged robots remains to be studied. The case where all the legs are not attached at the same point on a polygonal/polyhedral body is particularly relevant. A spider robot for which all the legs are not of the same length is also an interesting model.

Acknowledgments. We would like to thank Joseph O'Rourke for helpful comments.

REFERENCES

[1] J.-D. Boissonnat, O. Devillers, L. Donati, and F. Preparata, *Motion planning of legged robots: the spider robot problem*, Internat. J. Comput. Geom. Appl., 5 (1995), pp. 3–20.

[2] J.-D. Boissonnat, O. Devillers, and S. Lazard, *From spiders robots to half-disks robots*, in Proc. 11th IEEE Internat. Conf. Robot. Autom., 1994, pp. 953–958.

[3] ———, *Motion planning of legged robots*, in The First Workshop on the Algorithmic Foundations of Robotics, A. K. Peters, Boston, MA, 1994.

[4] ———, *Motion planning of legged robots*, Research Report 3214, INRIA, BP93, 06902 Sophia-Antipolis, France, 1997.

[5] M. Dickerson and R. L. Drysdale, *Fixed radius search problems for points and segments*, Inform. Process. Lett., 35 (1990), pp. 269–273.

[6] J. Hershberger, *Finding the upper envelope of n line segments in $O(n \log n)$ time*, Inform. Process. Lett., 33 (1989), pp. 169–174.

[7] S. Hirose and O. Kunieda, *Generalized standard foot trajectory for a quadruped walking vehicle*, The International Journal of Robotics Research, 10 (1991).

[8] S. Hirose, M. Nose, H. Kikuchi, and Y. Umetani, *Adaptive gait control of a quadruped walking vehicule*, in Int. Symp. on Robotics Research, MIT Press, 1984, pp. 253–277.

[9] J.Bares and W.L.Whittaker, *Configuration of an autonomous robot for mars exploration*, in World Conference on Robotics Research, 1989, pp. 37–52.

[10] K. Kedem and M. Sharir, *An efficient motion planning algorithm for a convex rigid polygonal object in 2-dimensional polygonal space*, Discrete Comput. Geom., 5 (1990), pp. 43–75.

[11] K. Kedem, M. Sharir, and S. Toledo, *On critical orientations in the Kedem-Sharir motion planning algorithm for a convex polygon in the plane*, Discrete Comput. Geom., 17 (1997), pp. 227–240.
[12] S. Lazard, *Planification de trajectoires de robots mobiles non-holonomes et de robots à pattes*, thèse de doctorat en sciences, université Paris 6, France, 1996.
[13] *Special issue on legged locomotion*, Internat. J. Robot. Res., 3 (1984).
[14] *Special issue on legged locomotion*, Internat. J. Robot. Res., 9 (1990).
[15] M. Sharir, *On k-sets in arrangements of curves and surfaces*, Discrete Comput. Geom., 6 (1991), pp. 593–613.
[16] S. Sifrony and M. Sharir, *A new efficient motion-planning algorithm for a rod in two-dimensional polygonal space*, Algorithmica, 2 (1987), pp. 367–402.
[17] V. Turau, *Fixed-radius near neighbors search*, Inform. Process. Lett., 39 (1991), pp. 201–203.